Title

Supercapacitors Performance Evaluation

Journal

Advanced Energy Materials, 5(6)

ISSN

1614-6832

Authors

Zhang, S

Pan, N

Publication Date

2015

DOI

10.1002/aenm.201401401

Peer reviewed

List of Figures

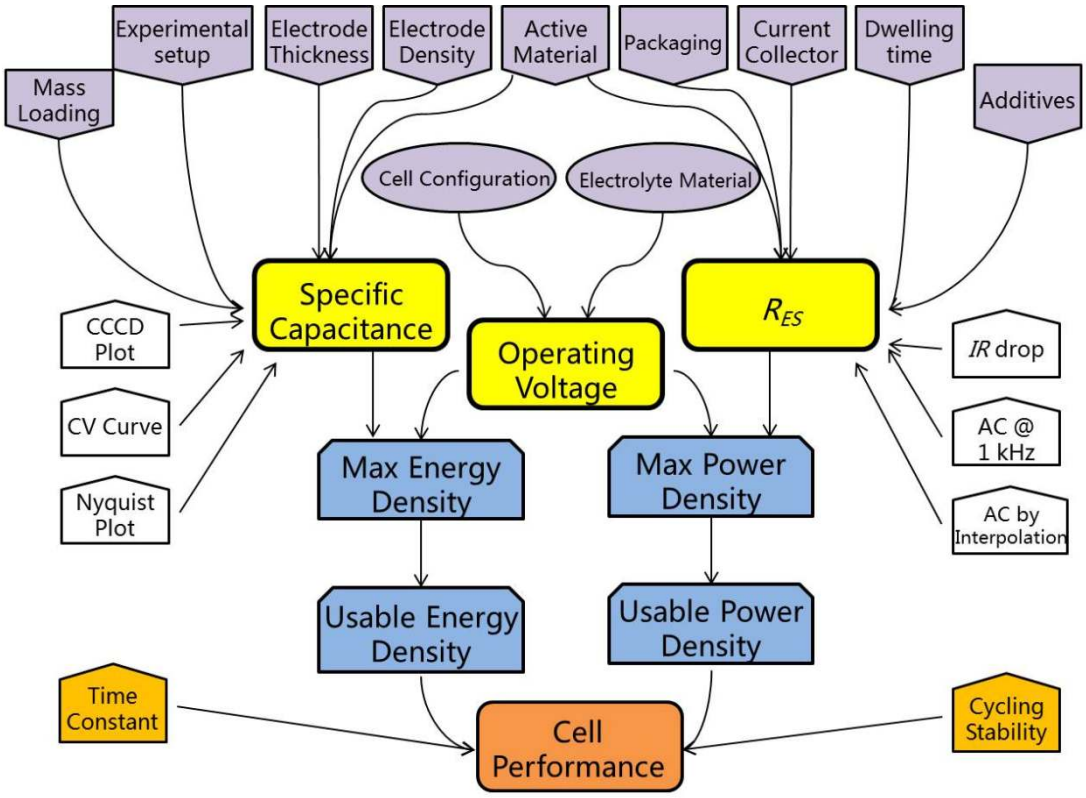

Figure 1. An illustration of key performance metrics, test methods, major affecting factors for the evaluation of SCs.

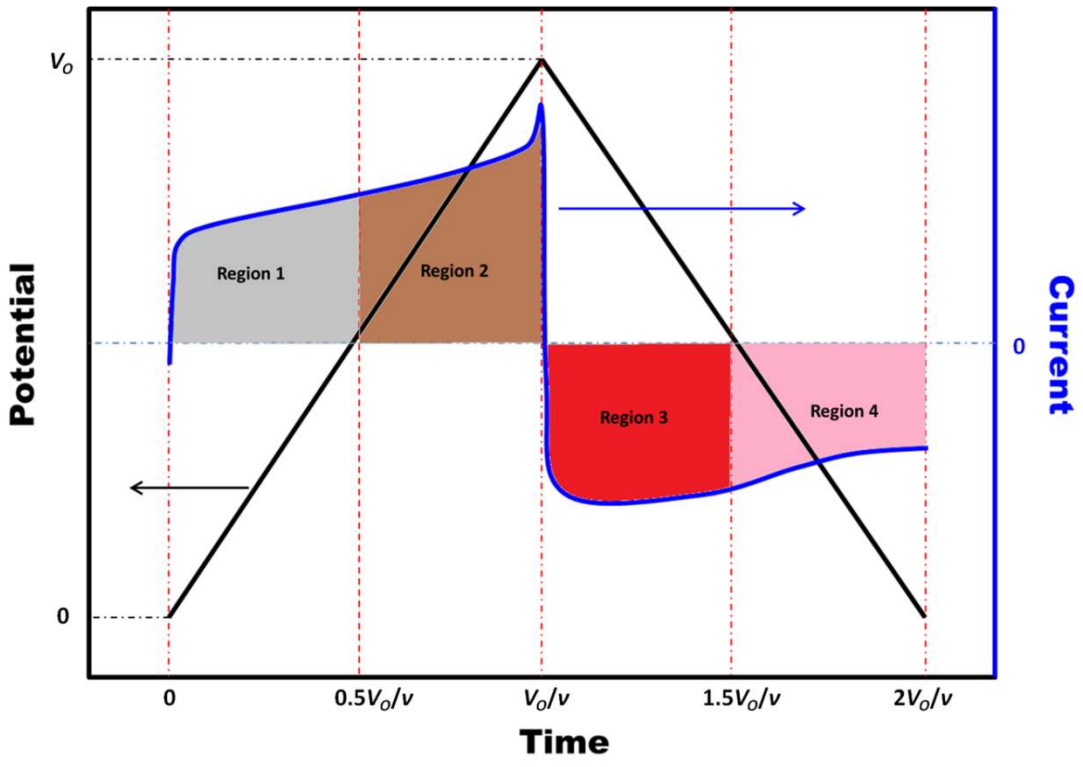

Figure 2. An illustration of a typical CV test result.

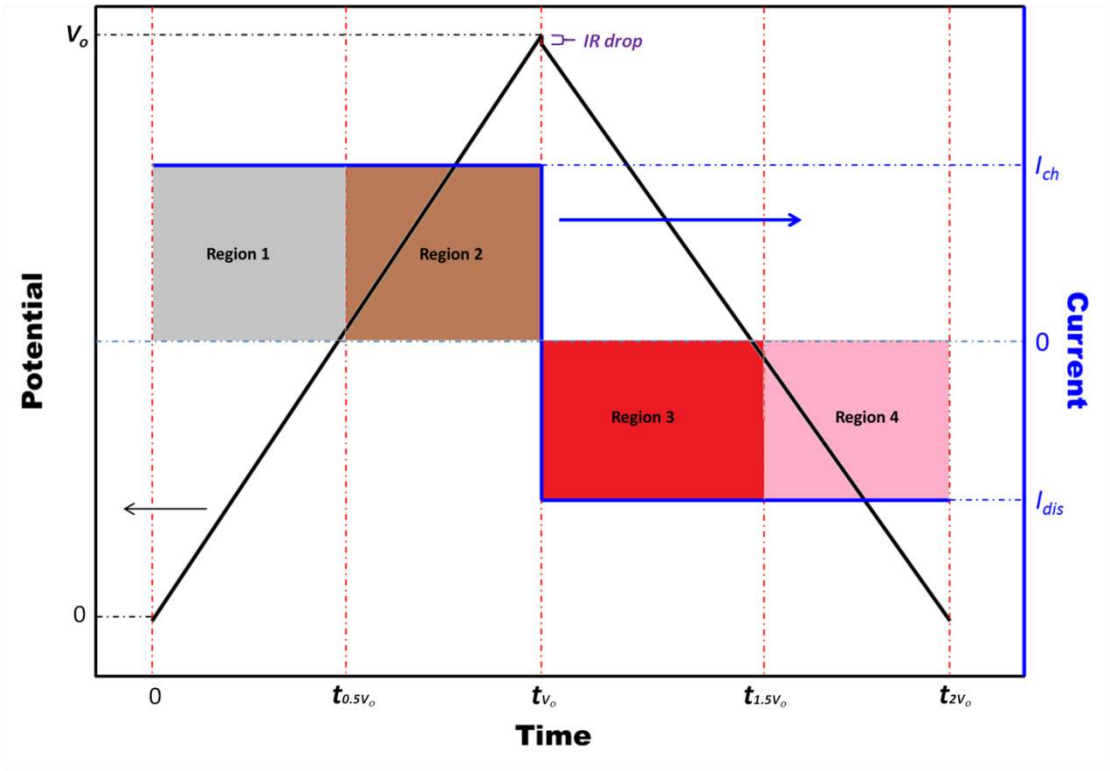

Figure 3. An illustration of CCCD test result with linear potential change over time.

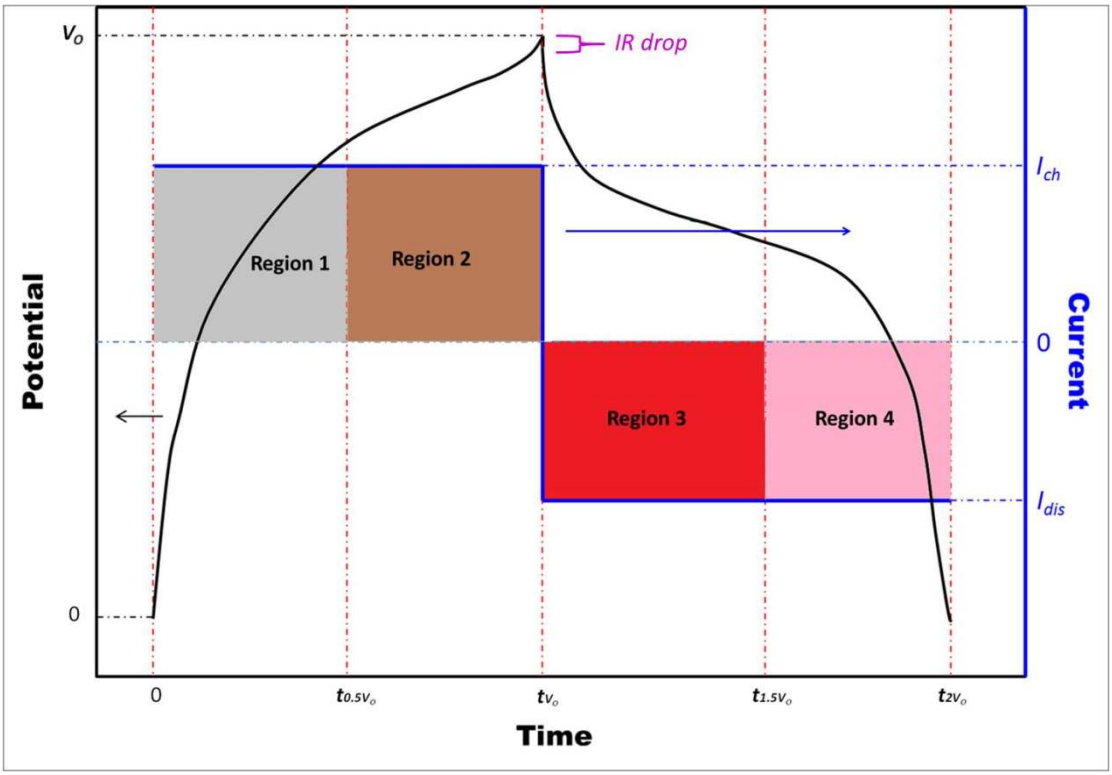

Figure 4. An illustration of CCCD test result with nonlinear potential change over time.

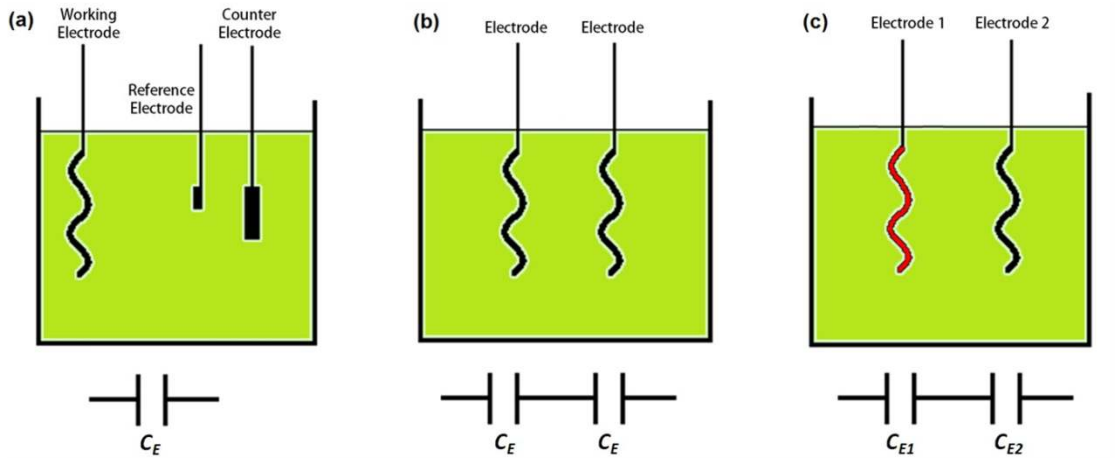

Figure 5. Schematic illustrations and equivalent circuits for different experimental setups.

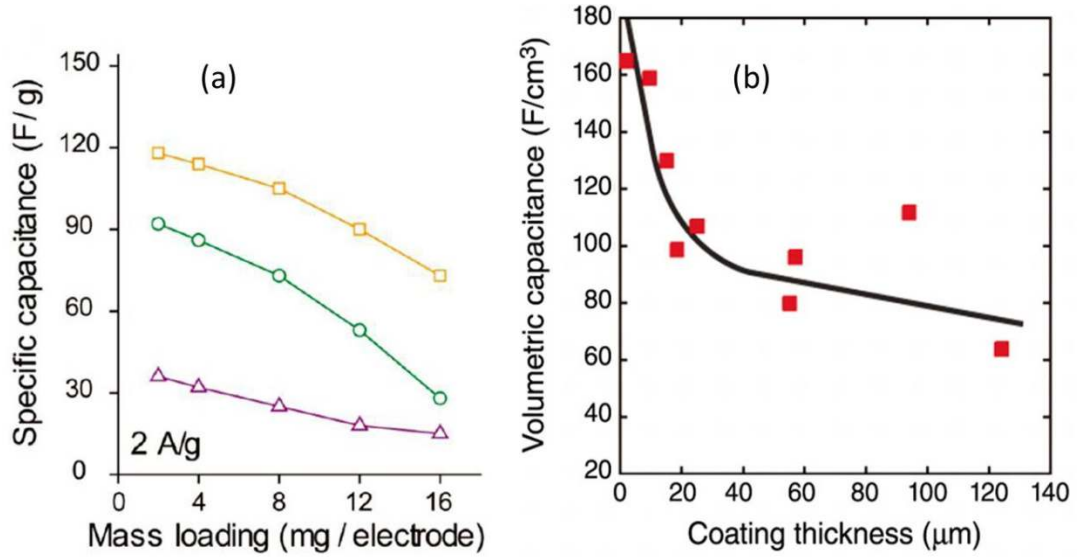

Figure 6. a) Effect of mass loading and b) electrode thickness on the resulting C_S: yellow squares, green circles and purple triangles represent crumpled graphene balls, wrinkled graphene sheets, and flat graphene sheets as electrodes; and red solid squares indicate carbide-derived carbons (CDCs) as electrodes [85, 150].

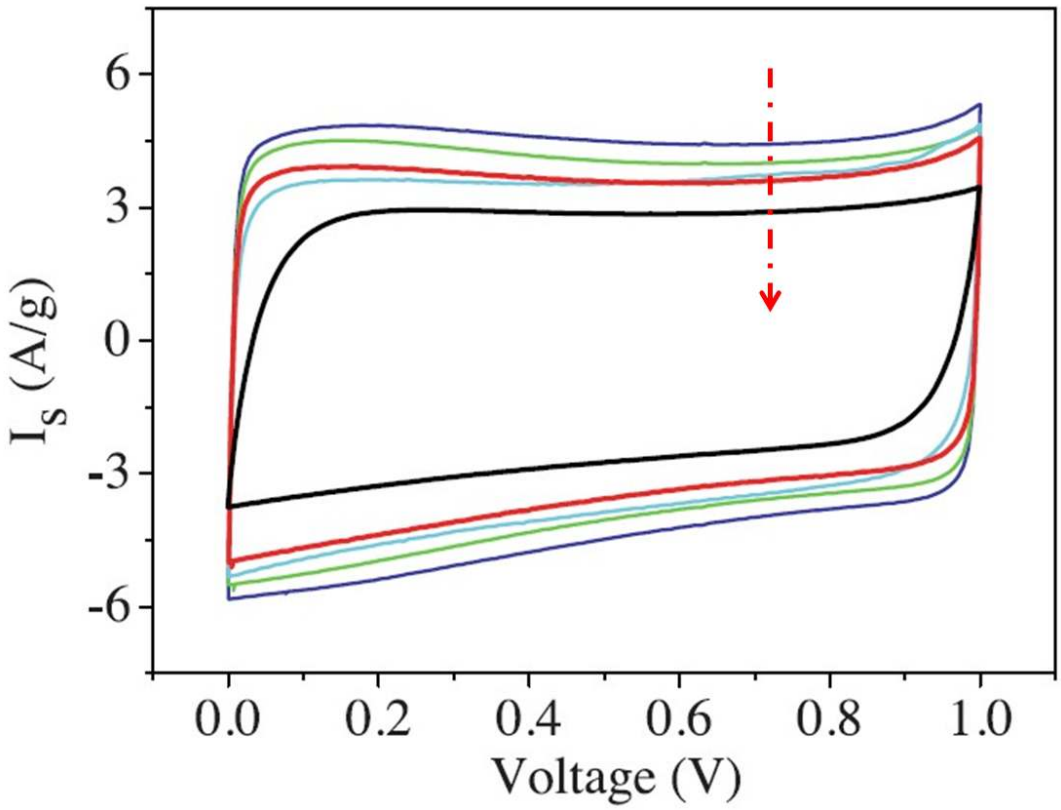

Figure 7. Cyclic voltammograms of liquid-mediated graphene materials with increasing electrode density from 0.13 to 1.33 g/cm^3 following the dashed red arrow [60].

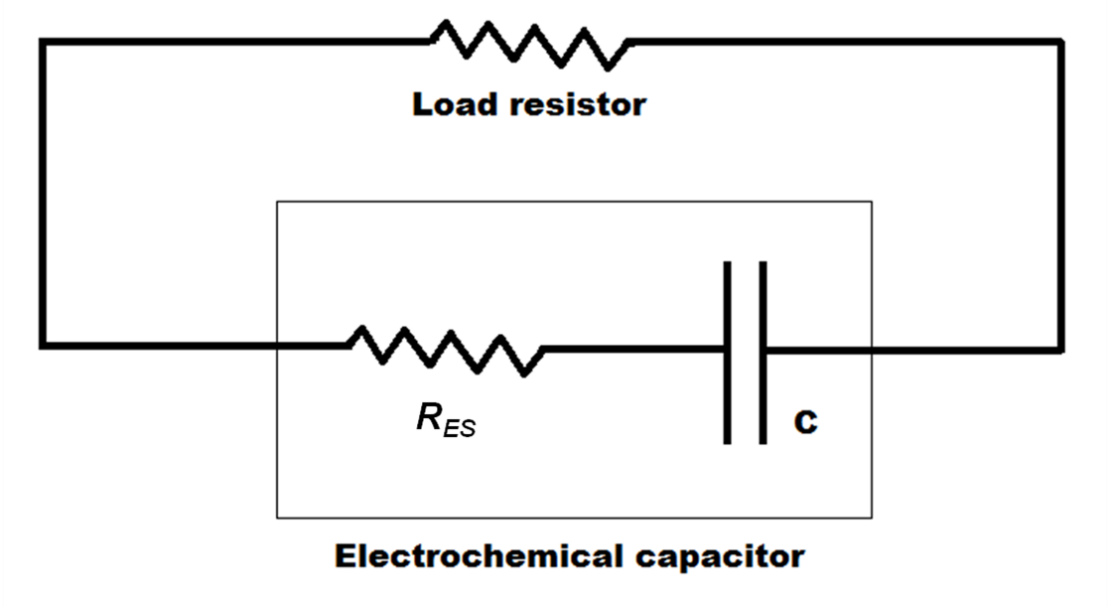

Figure 8. The series RC circuit for supercapacitors.

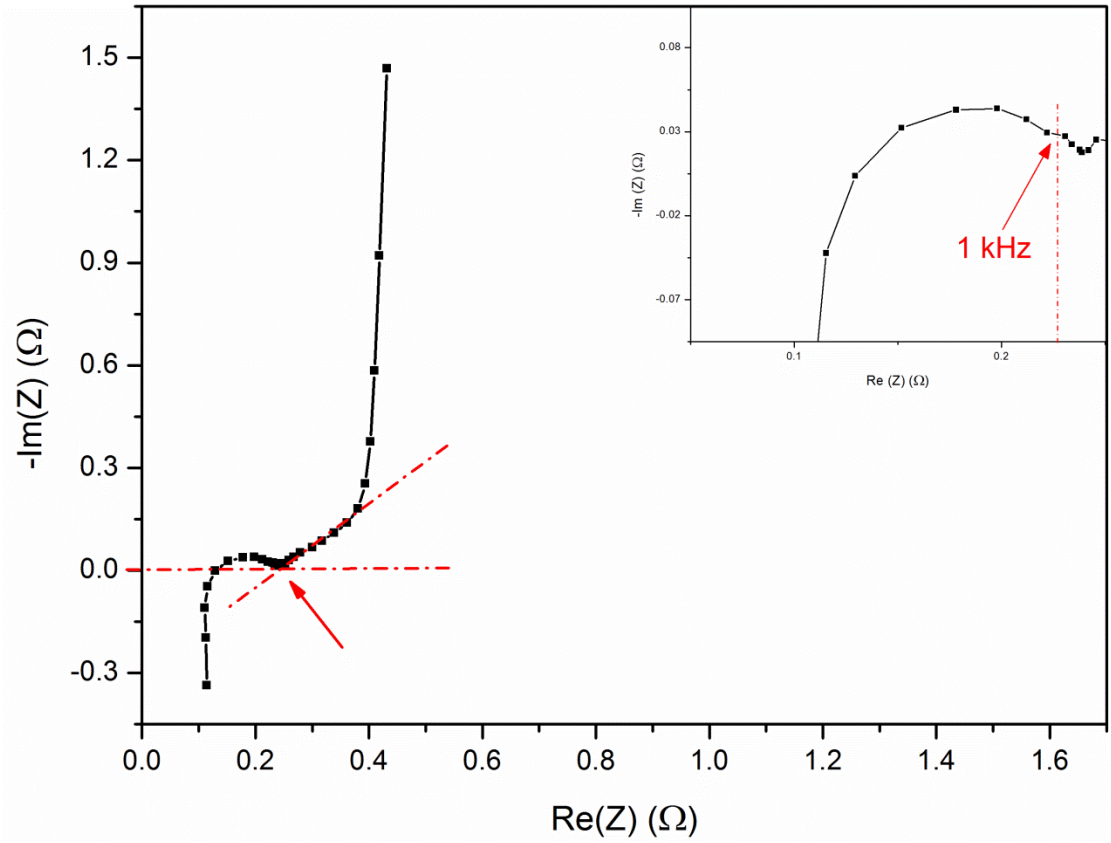

Figure 9. The Nyquist plot of 2.7V/1F Maxwell SC with R_{ES} determination methods marked in red.

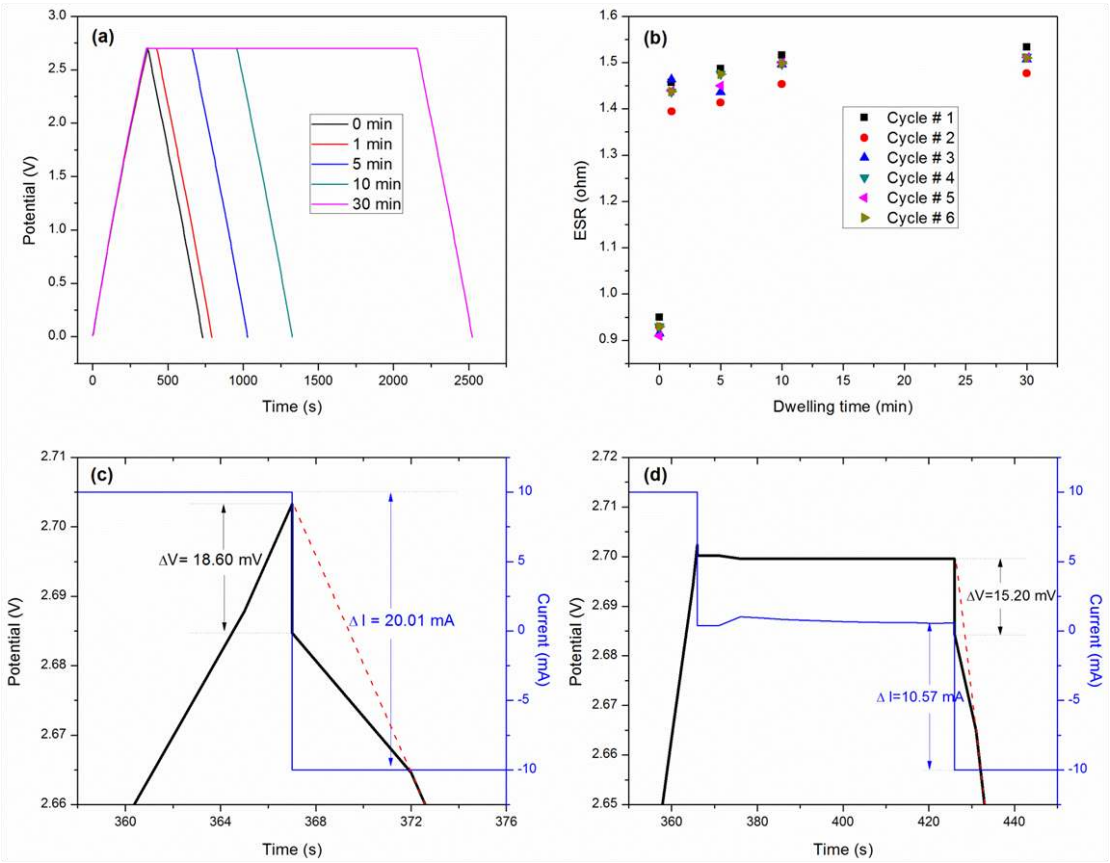

Figure 10. CCCD result of 2.7V/1F Maxwell SC tested at different dwelling time from 0 – 30 min: (a) overall CCCD plots of one cycle; (b) averaged R_{ES} values from first six cycles; enlarged upper region of the CCCD plots at dwelling time of (c) 0 min and (d) 1 min.

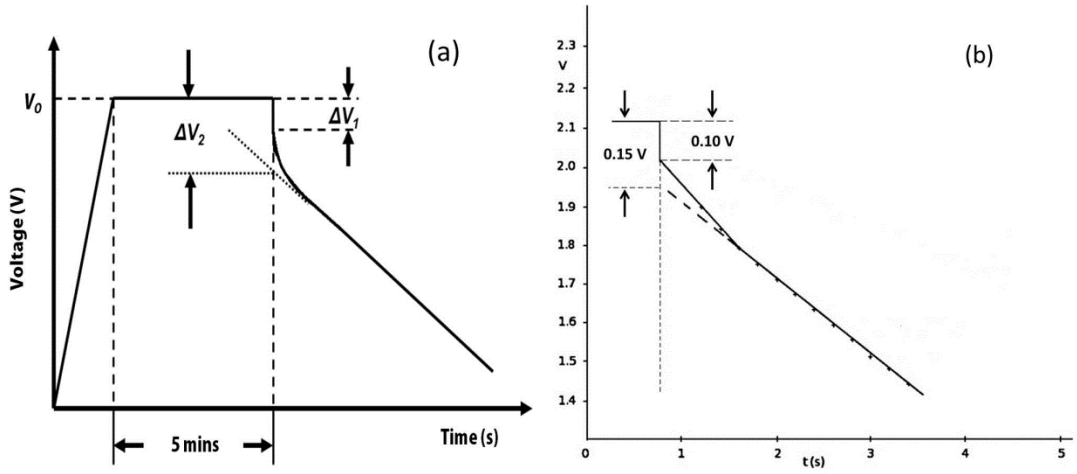

Figure 11. (a) A typical CCCD plot for large SCs with *IR* drop and steady-state voltage drop marked as ΔV_1 and ΔV_2, and (b) a real case illustration of the discharge part via Skeleton Tech 1600F SC.

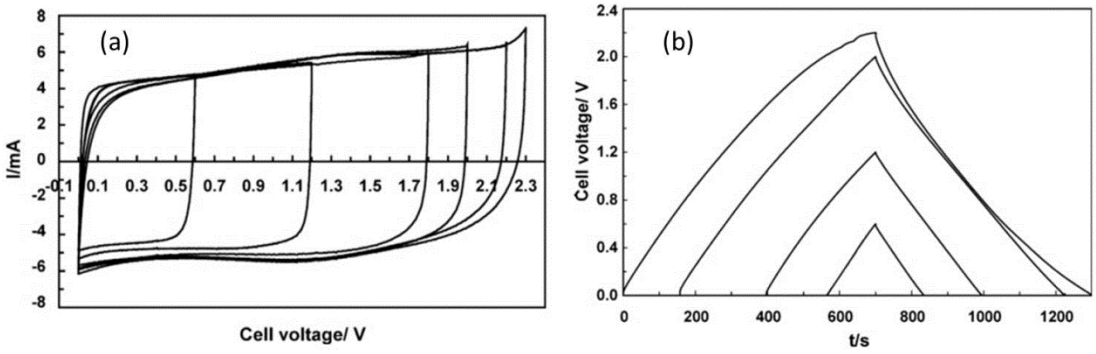

Figure 12. An illustration of V_o determination methods using (a) CV and (b) CCCD tests.

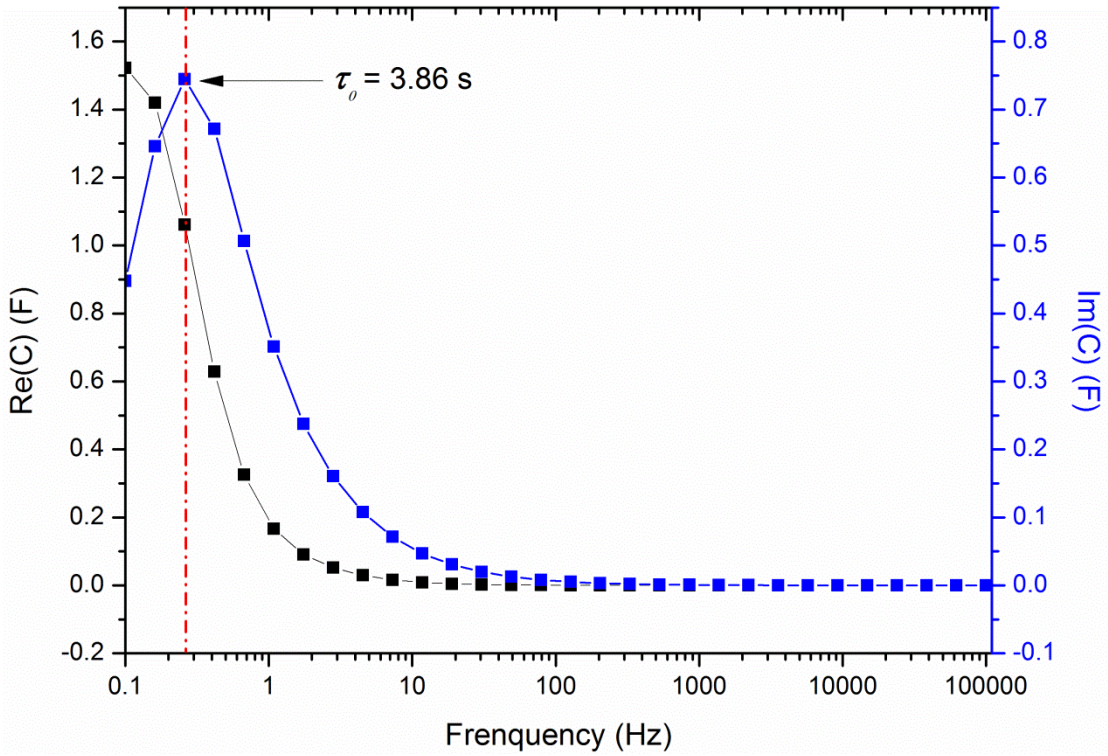

Figure 13. Dependence of real and imaginary capacitances over frequency for 2.7V/1F Maxwell SC with the relaxation time constant τ_o pointed.

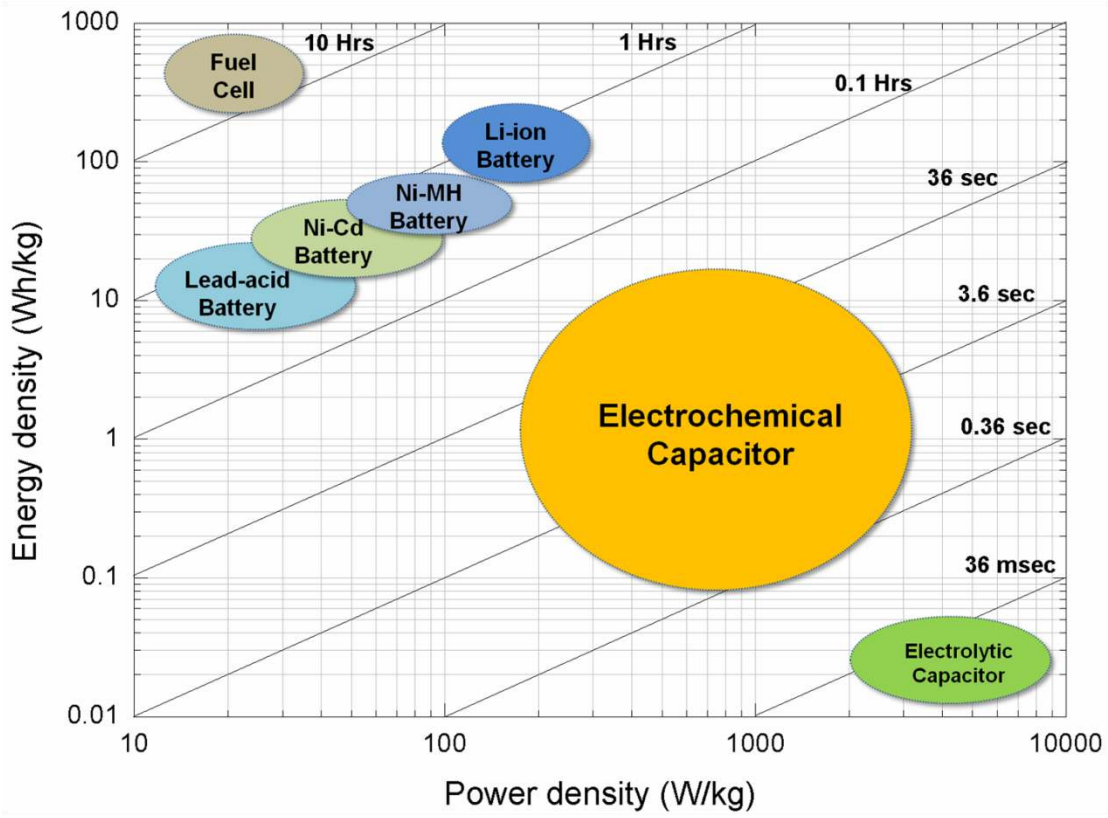

Figure 14. An illustration of the power and energy densities for several EES devices via Ragone plot. The plot is based on data from Ref. [114, 119-122].

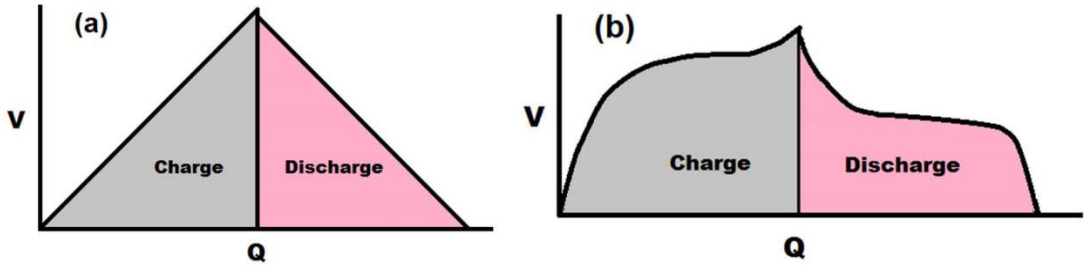

Figure 15. Representative working diagram from CCCD test for EDLCs (a), and PCs (b).

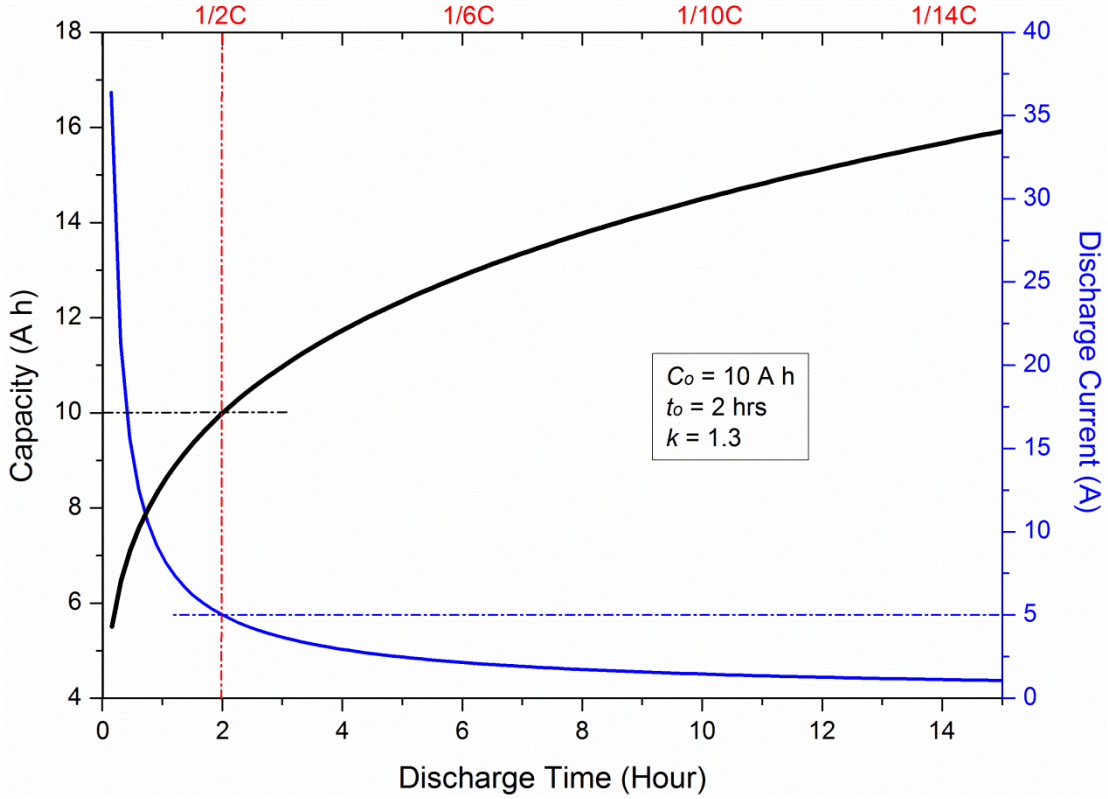

Figure 16. An illustration of Peukert's curve for batteries with the use of ½C marked by dashed lines.

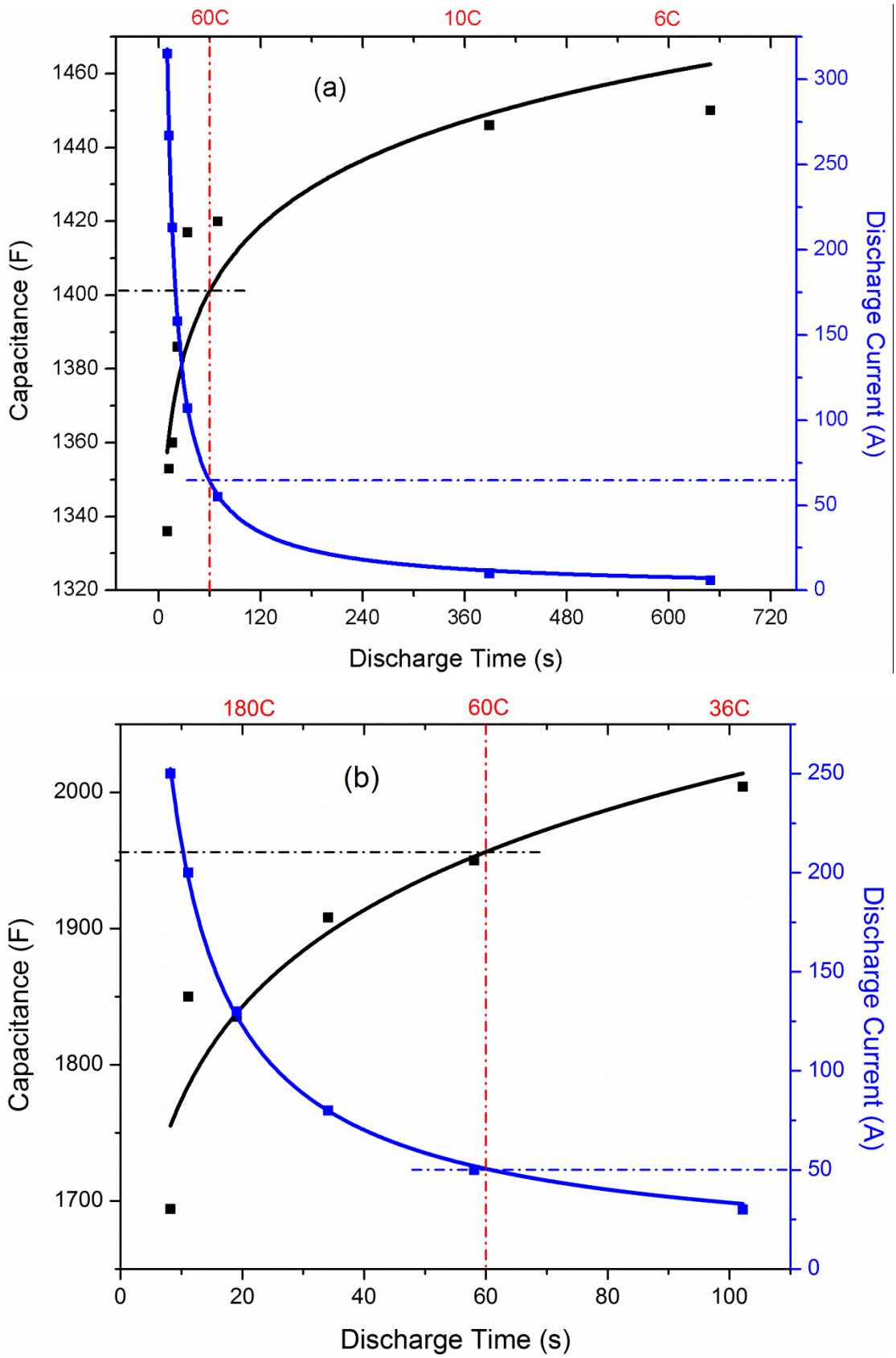

Figure 17. An illustration of Peukert's curves for a 1450F EDLC (a) and for a 2000F hybrid SC (b) with the use of 60C marked by dashed lines.

Supercapacitors Performance Evaluation

Sanliang Zhang and Ning Pan*

Department of Biological and Agricultural Engineering, University of California, Davis, CA 95616, United States

** Corresponding author: Tel.: +1 530 752 6232; fax: +1 530 752 7584*

E-mail address: npan@ucdavis.edu (N. Pan).

Keywords: Evaluation methods; *Inconsistencies*; Performance metrics; Supercapacitors.

Abstract

The performance of a supercapacitor can be characterized by a series of key parameters, including for instance the cell capacitance, operating voltage, equivalent series resistance, power density, energy density, and time constant. To accurately measure these parameters, a variety of methods have been proposed and used among academia and industry. As a result, some confusion has been caused due to the *inconsistencies* between different evaluation methods and practices. Such confusion hinders effective communication of new research findings, and creates a hurdle in transferring novel supercapacitor technologies from research lab to commercial applications.

Based on public sources, this review article is an attempt to inventory, critique and hopefully streamline the commonly used instruments, key performance metrics, calculation methods, and major affecting factors for supercapacitor performance evaluation. Thereafter the primary sources of *inconsistencies* are identified and the possible solutions are suggested correspondingly, with emphasis on device performance *vs*. material property and the rate dependency of supercapacitors. We hope, by using *reliable, intrinsic* and *comparable*

parameters produced, the existing *inconsistencies* and confusion can be largely eliminated so as to facilitate further progress in the field.

Table of Contents

1. Introduction

1.1. General power storage cells

The detrimental long-term effects of greenhouse gas emission into atmosphere and the finite supply of fossil fuels underscore the urgency of exploring renewable energy resources and the related energy generation, storage, and conservation technologies. A major hurdle, in general, lies in the dependence on the power line for electricity supply. The proposed wireless power supply [1, 2] is still largely at exploration stage and unlikely to play significant role in foreseeable future. The pending obstacle for use of renewable energy from wind and solar is the stability and quality of the produced electricity [3]. Driven by such need for power storage, rectification, transport and supply at various scales, sustained and extensive research and exploration have been conducted, and a number of electrical energy storage (EES) technologies have been developed so far; some have been serving very close to our daily life such as batteries and fuel cells, and others are more for industrial applications including pumped hydro, flywheel, compressed air, superconducting magnetic, and supercapacitors [4].

Of these EES technologies, batteries have been widely used at various scales, and have been continuously studied due to their outstanding performance. Based on the specific battery chemistry, they can be rechargeable or non-rechargeable. Both of them produce electricity from chemical energy via redox reactions at anode and cathode. For rechargeable batteries, they can reverse this process for certain times [5-7]. Starting in 20th century, batteries have been successfully penetrating into our daily life. However, there are certain areas where batteries revealed their shortcomings or failed to meet the needs, including:

- Low power density: This issue has severely hindered its applications where high power discharge and/or recharge rate is demanded;

- Safety issue: Many electrolytes used in batteries are corrosive, flammable, or both, and many electrodes are environmentally unfriendly or poisonous;
- Heat generation: The redox reactions in batteries may lead to Joule heating and thermochemical heating during their operation [8]. Such heat if not dissipated effectively will result in overheating, thermal runaway and even fire;
- Limited cycle life: The cycle lives of batteries are normally limited due to the nature of the redox reactions.

Because of the issues listed above, batteries alone are unable to provide the full solution for electricity storage. A durable and safe electricity storage device, with high power and/or energy performance, will undoubtedly transform the landscape of electric energy generation, distribution and utility. Besides, as consumer, industry and military require more compact and reliable electrical power systems, development of such devices continues to be one of the major thrusts in the area [9-11].

1.2. Supercapacitors and the charge storage mechanisms

Supercapacitors (SCs), often referred to as ultracapacitors or electrochemical capacitors, demonstrate outstanding power performance, excellent reversibility, very long cycle life (>1,000,000 cycles), simple mode of operation and ease of integration into electronics [12-20]. In addition, they generate less thermochemical heat because of the simpler charge storage mechanisms associated [21]. Therefore, they have been widely used in consumer electronics, memory back-up systems, and industrial power and energy management [5, 12] and will be found in more niche markets in the near future [22].

1.2.1. Charge storage mechanisms

It is generally accepted that there are three major charge storage mechanisms involved in the operation of SCs: (a) electric double layer in electric double layer capacitors (EDLCs); (b) highly reversible surface redox system, and (c) fast electrolyte ions intercalation, both occurring in pseudocapacitors (PCs).

a. Electrical double layer (EDL)

Electrical double layer (EDL) refers to the two charged layers formed at electrode/electrolyte interfaces [23]. The earliest model of EDL is usually attributed to Helmholtz [24, 25] and thus EDL is also termed as Helmholtz double-layers. Later on, Gouy-Chapman model and Gouy-Chapman-Stern model were developed to more accurately describe the detailed structure of EDLs [23, 26].

Electricity storage and delivery via EDL was first proposed by Becker in 1957 (U.S. Patent 2,800,616), and the resulting SCs is then named electric double layer capacitors (EDLCs). High-surface-area activated carbon (AC) is normally used in the system as the working medium. Owing to the huge surface area, EDLCs can store much more electricity, and are usually evaluated in Farads (F), whereas conventional dielectric and electrolytic capacitors are in picofarads (pF) and microfarads (μF).

b. Surface redox system

The second charge storage mechanism in SC was introduced by Trasatti [27], attributed to the highly reversible surface redox reaction, during which partial charge transfer between electrode and electrolyte occurs [28]. Normally during charging, the redox-active electrode

materials, i.e. RuO_2 or MnO_2, reduced to lower oxidation state coupled with adsorption of cations from the electrolyte. Upon discharge, the process can be almost fully reversed [29, 30]. Unlike EDLCs where the electrical charge storage is statically in the Helmholtz double-layers without any faradic charge transfer, such pseudocapacitors (PCs) do have partial faradic charge transfer at the interface between the electrode and electrolyte.

c. Ion intercalation

Another pseudocapacitive (PC) charge storage mechanism is a diffusion controlled intercalation process in which electrolyte ions migrate in and out of the atomic layers of electrode materials during charging and discharging [31]. This nevertheless differs from that of lithium-ion batteries by: 1) its excellent reversibility upon recharging [30]; 2) its state-of-charge dependent potential [32]. Various materials, e.g. molybdenum nitrides, niobium pentoxides and titanium carbides [33-35], have been examined for this purpose.

1.2.2. Overall charge storage ability and hybrid supercapacitors

In practice, the overall charge ability of a SC is enabled by two or three such charge storage mechanisms. They coexist in SCs and contribute in different proportions. For example, the charge storage of AC-based EDLCs is dominated by the formation of EDLs, but the oxygen-containing groups on AC surface might induce some surface-redox reactions.

Furthermore, hybrid or asymmetric capacitors by combining different electrodes of EDLCs and PCs, or even of batteries have been reported so as to improve the energy performance while maintaining their intrinsic high power performance [36]. The most widely acknowledged hybrid system is the Li-ion capacitor (LIC), normally produced by using

$Li_4Ti_5O_{12}$ nanocrystals [37-39] or advanced graphite materials [40] as positive electrode, and AC as negative electrode. Another one is called "ultrabattery" based on the combination of lead-acid battery and EDLC [41-44]. Indeed combination of high energy density of batteries with long cycle life and short charging times of supercapacitors is considered the likely future direction [45].

1.3. Performance evaluation for supercapacitors

To evaluate SCs performance, three essential parameters, cell (total) capacitance C_T, operating voltage V_o and equivalent series resistance R_{ES}, are often used to assess their energy and power performance, and usually are sufficient for commercial products where the materials, fabrication and cell design are all fixed. However in the research arena of constant probing for novel materials, more advanced manufacturing processes and new cell design, some other factors become indispensible. In fact, there is a rather large group of important factors necessary to paint the whole picture for supercapacitors, and a glance of the complex inter-relationship between the different performance metrics, the major affecting factors and the corresponding test methods is presented in **Fig. 1**. Several color schemes are employed in the figure: the three core parameters are highlighted in yellow; the power and energy densities in dark blue; time constant and cycling stability in light orange; all the important affecting factors in light purple; and the corresponding test methods in white. Note that the chart is more for illustration purpose and is by no means exclusive in presenting all the factors or detailing the complex multifaceted connections between them. For example, the evaluation method for V_o and the influence of electrolyte materials on specific capacitance are not explicitly presented.

Giving such multiple performance metrics, test methods, affecting factors shown in the figure, and the multifaceted relationships among them, *inconsistencies* become inevitable in the test results for the same cell measured in different labs, using different methods, and between academia and industry. To understand the causes for such *inconsistencies*, some important issues have to be addressed, including material property *vs*. device performance, and the rate dependency of supercapacitor performance.

Many attempts have been carried out to standardize the evaluation methods for SC devices. Some national and international bodies including DOD (US Department of Defense), DOE (US Department of Energy), IEC (International Electrochemical Commission), and SAE (Society of Automotive Engineers) have worked intensively on this matter. The resulting documents are summarized in **Table 1** chronologically.

Table 1. A chronological review of SC evaluation standards.

Year	Organization	Title	Document ID
1986	DOD	Capacitors, fixed, electrolytic, double layer, carbon (metric), general specifications	DOD-C-29501
1994	DOE	Electric vehicle capacitor test procedures manual	DOE/ID-10491
2004	DOE	FreedomCAR ultracapacitor test manual	DOE/NE-ID-11173
2006	IEC	Fixed electric double layer capacitor for use in electronic equipment	IEC 62391

2009	IEC	Electric double layer capacitors for use in hybrid electric vehicles – Test methods for electrical characteristics	IEC 62576
2012	IEC	Railway applications – Rolling stock equipment – Capacitors for power electronics – Part 3: Electric double-layer capacitors	IEC 61881-3
2013	SAE	Capacitive energy storage device requirements for automotive propulsion applications	J3051

Apparently, such efforts are mainly for specific applications oriented for industry, and there is still lacking a general understanding and knowledge collected/derived from the most recent cutting edge research so as to guide a more accurate and effective practice for performance evaluation of SCs. This prompts our intension to write this article.

In view of the urgent need for more reliable test methods called for by the drastic pace in searching for new energy storage solutions, and the complexities involved, this paper represents an attempt in clarifying and streamlining the existing evaluation methods, in the hope to eliminate/alleviate such *inconsistencies* and facilitate more effective communication in the field.

2. Instruments and measurements of key metrics

2.1. Instruments

Various instruments or test modes have been developed and applied to characterize the electrochemical performance of SCs. Cyclic voltammetric (CV), constant current charge/discharge (CCCD) and electrochemical impedance spectroscopic (EIS) tests are the commonly used ones. In essence, all such instruments can be used to measure the three fundamental parameters: voltage, current and time, and then other metrics, including the capacitance, equivalent series resistance, operating voltage and subsequently time constant, energy and power performance of SCs, can be derived from them. However, each of the instruments has its own focus and the targeted parameters by design, and their applications and limits are hence discussed below.

In addition, the three test modes can all be used to examine not only SC materials, i.e. the electricity storage media including electrode materials and electrolyte materials, but also SC devices, i.e. the whole package of SCs. Clear differentiation between a property measured for the cell or just for its active material has to be made when reporting a test result - a clearly logical practice yet often ignored. Also some technical differences exist when testing SC devices versus SC materials, and we will therefore stress this in our discussion.

2.1.1 CV

CV test applies a linearly changed electric potential between positive and negative electrodes for two-electrode systems, or between reference and working electrodes for three-electrode configurations. The speed of potential change in mV/s is termed as the sweep rate or scan rate, and the range of potential change is called potential window or operating potential. The instantaneous current during the cathodic and anodic sweeps is recorded to characterize the electrochemical reactions involved. The data are plotted as current (*A*) *vs*.

potential (*V*), or sometimes, current (*A*) or potential (*V*) *vs*. time (s) [26].

To examine the charge storage mechanisms of SC materials where EDLC and PC types are separate, CV test with the three-electrode setup is regarded as the most suitable approach [33, 34]. The test results can first be analyzed by examining the shape of the CV curves, as for EDLC materials, the resulting CV curve shape is rather rectangular, whereas for most PC materials, a sudden current surge appears to skew the curve. However, a complication in this is that there a few PC materials [35] whose CV curves also appeared rectangular. To add a further twist, the shape of the CV curves can be affected by the experimental setup [46] so that some PC materials, which ordinarily would generate skewed CV curves, can produce rectangular curves as well. Caution is hence required in the process.

Another more quantitative and reliable method in interpreting the data from a SC cell tested is to extract the contributions from EDL and PC mechanisms separately by utilizing the knowledge that the instantaneous current induced by EDL mechanism is proportional to the scan rate, while the diffusion controlled ion-intercalation by PC mechanism is to the square root of scan rate [33, 34, 47-51]. However, this approach is limited to detect the contribution from the surface-redox mechanism. Therefore, more experimental and theoretical studies are demanded to address this issue.

CV test is also particularly suitable in practice to determining the potential window (operating voltage) for SC materials by successive adjustment of the reversal potential in a three-electrode system, and the reversibility of the charge and discharge processes can also be studied at the same time [32, 33]. In addition, the specific capacitance and energy performance of the SC materials can be obtained via integration of the CV curves as discussed in detail later. Similar process can also be conducted for SC devices to obtain their

total cell capacitance and hence the amount of electricity stored.

2.1.2 CCCD

CCCD test is the most widely used method for characterization of SCs under direct current [52, 53]. It is conducted by repetitive charging and discharging the SC device or the working electrode at a constant current level with or without a dwelling period (a time period between charging and discharging while the peak voltage V_o remains constant), and normally a plot of potential (E) *vs*. time (s) is the output. Choosing a proper level of the constant current is critical to produce consistent and comparable data from a CCCD test.

CCCD test is regarded as the most versatile and accurate approach in characterizing SC devices. All three core parameters of SC devices, C_T, R_{ES} and V_o, can be tested from it and subsequently used to derive most of the other properties, such as the time constant, power and energy densities, and leakage and peak current. It can also be conveniently used to study the cycling stability of SC devices. Moreover, by using a three-electrode setup, the specific capacitance, reversibility and potential window for SC materials can also be obtained via CCCD test.

2.1.3 EIS

EIS test, also known as the dielectric spectroscopic test, measures the impedance of a power cell as a function of frequency by applying a low-amplitude *alternative* voltage (normally 5 mV) superimposed on a steady-state potential. The resulting data is normally expressed graphically in Bode plot to demonstrate the cell response between phase angle and frequency, and in Nyquist plot to show the imaginary and real parts of the cell impedances on

a complex plane [54, 55].

Besides the frequency response and impedance, EIS has also been employed to characterize the charge transfer, mass transport and charge storage mechanism, as well as to estimate the capacitance, energy and power properties [56, 57]. Different equivalent circuits and models have been developed to distinguish the contribution of individual structure component in a cell system to the total impedance [40, 58, 59]. When SC devices are tested, the real parts of the complex impedance at selected frequencies are used in literature to represent R_{ES}. However, one needs to keep in mind that this R_{ES} from EIS test is often much smaller than that derived from the CCCD test [60], and therefore is limited in describing the power performance of SC devices.

For SC materials, EIS test can be deployed to study the impedance, specific capacitance, charge transfer, mass transport and charge storage mechanisms involved by executing similar analysis in a three-electrode system.

2.2. Capacitance

The total capacitance C_T of a SC is a reflection of the electrical charge ΔQ stored under a given voltage change ΔV:

$$C_T = \frac{\Delta Q}{\Delta V} \qquad (1)$$

This is preferred when specifying the total charge storage ability of SC devices. A more intrinsic *specific* capacitance C_S is defined to measure, preferably, the charge storage ability of SC materials:

$$C_S = \frac{\Delta Q}{\Delta V \times \Pi} \qquad (2)$$

where Π can be the mass, volume, surface area of the electrode or the active material, or even

the size of the electrode, and the resulting specific capacitance C_S is often named correspondingly as the gravimetric capacitance (F/g), volumetric capacitance (F/ml), normalized capacitance (μF/cm^2) and areal capacitance (F/cm^2) or linear capacitance (F/cm). Sometimes, C_S is also used to describe device performance, when normalized by the whole cell weight or volume [61]. Note that although C_S is considered the most important parameter in comparing the charge storage ability of SC *materials*, **it is rarely mentioned by industry, as most of the commercial SCs are activated carbon (AC) based, and its C_S is generally considered a constant between 100 F/g and 70 F/cm^3 in organic electrolyte [62]. However, for scientists in searching for new materials, C_S is the more informative way to depict the charge storage ability of a given material.**

2.2.1 Evaluation of C_T

a. CV

The total capacitance C_T of a cell in **Eq. 1** can be further expressed as:

$$C_T = \frac{\Delta Q}{\Delta V} = \frac{\int_0^{2V_O/\nu} |i| dt}{2V_o} \qquad (3)$$

Through the integration of the resulting CV voltammograms, the accumulated charge as a function of potential can be obtained. Normally, the whole curve is recommended to use [63-67] as shown in **Eq. 3**. However in practice, different segments of the curve, as depicted in **Fig. 2** in distinctive colors, have been used in integration [46, 68-70], thus leading to *inconsistencies* in test results [46, 65, 66, 71-73]. It is worthy reminding that the potential change in Eq. 3 $\Delta V = 2V_o$ (0 to V_o and back to 0), for there are mistakes made in ΔV values [74-77].

b. CCCD

Since constant current is used in a CCCD test, **Eq. 1** can be converted to:

$$C_T = \frac{I * \Delta t}{\Delta V} \qquad (4)$$

where I is the constant current, Δt is the charging or discharging time corresponding to the specified potential change ΔV. **So the key issue now is that the correct time Δt and ΔV are used in calculation.** Often the entire discharging curve is used:

$$C_T = \frac{I_{dis} * \Delta t_{V_o - 2V_o}}{V_o} \qquad (5)$$

Since *IR* drop is inevitable in CCCD test, one can adjust ΔV so as to exclude the *IR* drop for more accurate result*, i.e.,*

$$C_T = \frac{I_{dis} * \Delta t_{V_o - 2V_o}}{V_o - V_{IR\,\mathrm{drop}}} \qquad (6)$$

Similar to CV test, different segments of the CCCD plots, as illustrated in **Fig. 3,** have been used in computing the cell capacitance [66, 70, 78]. Only this time as the current remains constant, identical C_T value is obtained regardless of the segment used, so long as the voltage changes linearly with time as in **Fig. 3**.

Whereas for PCs or hybrid SCs with nonlinear curves as seen in **Fig. 4**, the selection of different regions from the curve can make a great difference in determining ΔV, and hence C_T [79-82]. In such cases, the use of a proper or fixed region or selection of suitable potential window becomes critical and needs to be standardized. Based on Burke [53], Region 3 or a potential window from V_o to the shoulder voltage is recommended. Likewise, one can also

adjust ΔV to eliminate the *IR* drop to improve accuracy.

c. EIS

The conventional method of deriving capacitance from EIS test is based on the imaginary part of the complex impedance *Im(Z)* as shown in Eq. 7 [7, 54, 83]:

$$C_{Tf} = -\frac{1}{2\pi f \times Im(Z)} \qquad (7)$$

where *f* is the frequency. Normally this frequency is identified at which the phase angle reaches - 45 degree [83], or simply as the lowest frequency applied [7].

Another method introduced by Simon [56] is as below:

$$Re(C) = \frac{-Im(Z)}{\omega |Z|^2} \qquad (8)$$

$$Im(C) = \frac{Re(Z)}{\omega |Z|^2} \qquad (9)$$

where $Z = \sqrt{Re(Z)^2 + Im(Z)^2}$ is the overall complex impedance, $\omega = 2\pi f$ is angular velocity, *Re(Z)* is the real part of the complex impedance, and *Re(C)* and *Im(C)* are the real and imaginary capacitances, respectively. ***Im(C)* is a term related to the energy dissipation of the cell, and *Re(C)*, calculated at the lowest-frequency applied, indicates the energy stored, thus can be used to represent C_T** [56]**.**

2.2.2 Evaluation of C_S

Once C_T is obtained, the corresponding C_S can be calculated using Eq. 4. This seemingly straightforward step is made complicated by the fact that there is no established standard procedure in determining the base value for Π, be the mass, volume, or other quantity. **A mediocre C_T value can lead to an excellent C_S if a sufficiently small Π is used.** For this

reason, along with other possible considerations, technical or cost related, although attractive C_S results are frequently reported [74-77, 79-82], few have been successfully transferred to commercial products. **One solution to this problem is that both C_T and the corresponding C_S values, as well as the Π value, be explicitly reported side by side.** Besides Π, other factors as discussed in next section, including experimental setup, mass loading and electrode thickness, and electrode density, can also alter C_S value dramatically [65, 84, 85] and therefore recommended to be reported as necessary information.

2.2.3 Major affecting factors

a. Experimental setup

Study has demonstrated that quite different C_S values can be obtained for the same SC electrode when different experimental setups are adopted [46]. The three major experimental setups: symmetric two-electrode, asymmetric two-electrode and three-electrode configurations, are illustrated in **Fig. 5**. The three-electrode one is particularly useful in accurately determining the C_S for SC materials, and the two-electrode ones are normally used in SC device prototypes or final products. It is worth noting that it is also possible [86] to insert a reference electrode in the two-electrode system to study the detailed potential change in other two electrodes, but this scenario is not included here and the three-electrode configuration mentioned in this article solely means the setup presented in **Fig. 5a**.

The following analysis demonstrates how different setups can lead to different results. For brevity the gravimetric C_S is used. The weight of each individual electrode in **Figs. 5a** and **b** is assumed to be m, while m_1 and m_2 are for the two different Electrodes 1 and 2 in **Fig.**

5c. Assigning the single electrode capacitance as C_E, the gravimetric C_{Sa} in the three-electrode system can be calculated as [59]:

$$C_{Sa} = \frac{C_E}{m} \qquad (10)$$

For the symmetric two-electrode system shown in **Fig. 5b**, the cell total capacitance C_{Tb} can be obtained through:

$$\frac{1}{C_{Tb}} = \frac{1}{C_E} + \frac{1}{C_E} \qquad (11)$$

By counting the mass for both electrodes, hence:

$$C_{Sb} = \frac{C_{Tb}}{2m} = \frac{1}{4}(\frac{C_E}{m}) \qquad (12)$$

That is, even with identical SC material, **the *specific capacitance* obtained from the three-electrode system actually quadruples that from the symmetric two-electrode system**, i.e.,

$$C_{Sa} = 4 \times C_{Sb} \qquad (13)$$

This relationship has been validated experimentally by Béguin *et al* [46].

For the asymmetric two-electrode system in **Fig. 5c**, the cell capacitance C_{Tc}:

$$\frac{1}{C_{Tc}} = \frac{1}{C_{E1}} + \frac{1}{C_{E2}} \qquad (14)$$

Again by counting the mass for both electrodes, there is:

$$C_{Sc} = \frac{C_{Tc}}{m_1 + m_2} = \frac{1}{m_1 + m_2} \times \frac{C_{E1} \times C_{E2}}{C_{T1} + C_{T2}} \qquad (15)$$

In this configuration, normally the electrode capacitances of the two electrodes are balanced to fully unitize the charge storage ability of the SC material, i.e., $C_{E1} = C_{E2} = C_E$. So by employing other active material like pseudocapacitive one, it is normally accepted that the *specific* capacitance of Electrode 1 is larger. Conversely if the two electrodes achieve the same capacitance C_E, then less mass is needed in Electrode 1, say at a fraction α (**0< α <1**) of Electrode 2, so that $m_1 = \alpha m$, $m_2 = m$. Substituting them into **Eq. 15** yields,

$$C_{Sc} = \frac{1}{2(1+\alpha)} \frac{C_E}{m} \qquad (16)$$

Combined with **Eqs. 10** and **12**, there are:

$$C_{Sa} = 2(1+\alpha) C_{Sc} \qquad (17)$$

and

$$C_{Sb} = \frac{(1+\alpha)}{2} C_{Sc} \qquad (18)$$

Thus the three equations show distinctive results when using setup a, b or c. For example, if the *specific* capacitance in Electrode 1 doubles that in Electrode 2, α = 0.5 at the same potential window. Then there is $C_{Sa} = 3C_{Sc}$ and $C_{Sb} = 0.75C_{Sc}$!

It is worth noting that for SC devices, the *total capacitances* for symmetric and asymmetric are identical under the same assumptions:

$$C_{Tb} = C_{Tc} = \frac{1}{2} C_E \qquad (19)$$

The advantages of using asymmetric systems include first, as discussed below in 2.4.2, by using hybrid electrodes hence an asymmetric system, additional electrochemical potential

difference can be introduced so that the operating voltage of the cell can be boosted [72]. The second benefit is that for the same total capacitance, in an asymmetric system, the electrode of better PC material can cut the material use by a fraction (1-α) as demonstrated above. This can be significant if this PC material is so superior that α is small. However so far, the symmetric SC devices still demonstrate better power performance, and consequently play a dominant role in the market, despite the intensive study on asymmetric systems [72, 80, 87-92].

b. Mass loading and electrode thickness

Mass loading is defined as the mass of active material per unit area of the electrode, and electrode thickness is the net thickness of the active material on the current collector. These two parameters reflecting the fabrication process significantly impact the resulting C_S, but are often not specified. **Many studies used a very small mass loading or electrode thickness in calculating the specific capacitance C_S, and the resulted C_S appears outstanding in number but is often not meaningful in practice [93, 94]**. In general, it is suggested [65] that the mass loading to be at least 5 mg/cm^2 and the electrode thickness between 50 – 200 μm. Exceptions may be found for micro-supercapacitors [85, 94, 95] in special applications. **Fig. 6a** and **b** are two verifications showing the significant impact of them on C_S.

c. Electrode density

The electrode density describes how densely the electrode materials are packed on current collector, and is expressed in mass/volume. Although it is related to both mass loading and electrode thickness, there is the material density involved. It is reported that the

same electrode material with different packing densities can significantly influence the resulting electrochemical performance, including C_S, energy and power densities. Based on the targeted applications, there is an optimal level for the electrode density, so that the electrode is not over densely packed as to reduce the accessibility of SC materials, nor is it excessively loose to affect the volumetric performance. An example of its impact is provided in **Fig. 7** by using certain graphene materials with increasing densities from 0.13 to 1.33 g/cm^3 [61].

2.3. Equivalent series resistance

A SC is not an ideal electrical component in the sense that it has its own internal resistance, thus dissipating the energy stored. A SC cell can be simply treated as a system of a capacitor in series arrangement with a resistor R_{ES} in **Fig. 8**. The resistance of this resistor is usually termed as the equivalent series resistance, R_{ES}, and is essential in reflecting the power performance and energy efficiency of SCs. In general, a small R_{ES} is preferred for better electrochemical performance. Note that in actual measurement, only a packed cell can give an accurate R_{ES} value. It is because of this, whenever R_{ES} is referred to in this paper, it deals with a device not the material.

2.3.1 Evaluation of R_{ES}

a. CCCD

The most widely accepted method to evaluate R_{ES} is through the analysis of the *IR* drop or voltage variation at the initial stage of the discharging curve from CCCD tests. By

applying Ohm's law to the *IR* drop, R_{ES} can be acquired readily:

$$R_{ES} = \frac{\Delta V}{\Delta I} \qquad (20)$$

where ΔV and ΔI are the voltage and current of the *IR* drop, respectively.

Another less common approach is based on the voltage recovery behavior after a current interruption during a discharge process [96, 97]. This method is fundamentally the same as the *IR* drop method and yields matching results, and is hence not described in detail here.

b. EIS

Typically, the R_{ES} from EIS test is evaluated using the real part of the complex impedance at 1 kHz and is normally noted in Nyquist plot. Another method, via linear interpolation of the low-frequency part of Nyquist plot to $Im(Z) = 0$, is also used sometimes in literature. An example is provided in **Fig. 9** to illustrate these two methods in EIS test, testing a typical commercial SC, 2.7V/1F Maxwell cell. Compared to the R_{ES} derived from CCCD test, the value from EIS test is normally smaller.

2.3.2 Major affecting factors

There are two major factors that affect the accuracy of R_{ES} from CCCD test: the dwelling time and the size of SC. Normally, CCCD test is carried out without dwelling at peak potential, that is, the discharging starts once the peak potential is reached. However, the practice of non-zero dwelling time is widely adopted in tests, which can greatly influence the final value of R_{ES}. A couple of different dwelling time have been reported: 1 min in the procedure developed by Burke [98], 5 min in Illinois Capacitors [99], 10 min by Ioxus, [100]

etc. Another often overlooked affecting factor on R_{ES} is the size of SCs in terms of cell capacitance as defined in **Table 2**. The two factors are discussed in detail below.

Table 2. Defined SC size based on total cell capacitance.

	Micro cell	Small cell	Medium cell	Large cell	Ultra-large cell
C_T	< 1 mF	1 mF – 10 F	10 F – 100 F	100 F – 1000 F	>1000 F

a. Dwelling time

To the best of our knowledge, there is no study carried out to examine the influence of dwelling time on R_{ES}. Therefore, by using the same 2.7V/1F SC from Maxwell Technologies, we acquired and presented its CCCD plots with different dwelling time varying from 0 – 30 minutes in **Fig. 10a**. **Fig. 10b** demonstrated the impact of dwelling time on the resulting R_{ES}. To clearly display the variation of CCCD plots, we selected and enlarged the upper region of the plots with dwelling time of 0 min and 1 min, and showed them separately in **Fig. 10c** and **d,** with the potential and current changes marked in black and blue, respectively. If I is the constant current applied, then in the case of 0 min dwelling time, the current change is:

$$\Delta I \cong 2I \quad (21)$$

Whereas in the cases of > 0 min dwelling time,

$$\Delta I \cong I \quad (22)$$

Combined with the potential change, as charted in **Fig. 10b**: we have at 0 min dwelling time,

a much smaller R_{ES} ~0.93 ohms, compared to 1.47 ohms from dwelling time >0 min cases.

b. Cell size

It is still not clearly understood how the cell size affects the CCCD results. But it is generally accepted that the *IR* drop method works fine only for small SCs, and a steady-state voltage drop method should be used for large SCs. As shown in **Fig. 11a**, the steady-state voltage drop ΔV_2, rather than the *IR* drop ΔV_1, is obtained through the back extrapolation of the potential trace; it is larger than ΔV_1 by almost 50%, thus leading to a nearly 50% increase in R_{ES}. An actual example is provide in **Fig. 11b** reported in Ref. [53]. Studies [53, 101] have been conducted and the results demonstrated that more accurate power performance can be estimated using ΔV_2 for large cells, and it is therefore recommended.

2.4. Operating voltage V_o

Strictly speaking, the operating voltage $\boldsymbol{V_o}$ refers to the potential applied to the system or the suitable potential window within which a cell normally operates. In this paper, the term is sometimes interchangeable to cell voltage or rated potential, which represents the maximum voltage a cell can endure.

2.4.1 Evaluation of V_o

Both CV and CCCD tests can be used to determine V_o of either the SC materials or the devices. However actual test of this maximum potential can be risky of destroying the cell. An expedient method is normally applied, with an example given in **Fig. 12** using an asymmetric MnO_2/AC capacitor [72], where V_o can be achieved by starting with a lower

voltage applied to the cell, and then slowly increasing the voltage until a spike appears as seen in the figure.

2.4.2 Major affecting factors

Two major factors affecting V_o for SC devices include the solvent in electrolytes and the cell configuration. Normally, in aqueous systems, a cell can be charged to 1.0 V, limited by the thermodynamic decomposition potential of water at room temperature. V_o in organic solvent electrolyte varies between 2.3 – 2.7 V [21, 102-106]. As both energy and power densities are proportional to V_o^2, much effort has been dedicated to develop novel electrolyte that can endure high voltage (>3 V). Room temperature ionic liquid (RTIL) is considered to be the most promising candidate by which high V_o values between 3.0 – 6.0 V have been achieved in research labs [107, 108]. In addition, various mixtures of different RTILs, or RTIL and organic solvents, also appear to be attractive [109, 110].

The other factor influencing V_o is the cell configuration. In an asymmetric system, V_o can be increased by using different SC materials so as to introduce additional electrochemical potential difference [72]. This way, even in aqueous systems, V_o can reach 2.0 – 2.3 V [29, 72, 111, 112], giving rise to much improved energy storage [29, 113].

In conclusion, for SC materials, all three techniques, i.e. CV, EIS and CCCD tests, can be employed with different emphases. However, for SC devices, the most effective and accurate approach is CCCD test for measuring the cell capacitance, equivalent series resistance and operating voltage [53]. Subsequently, the time constant, energy and power densities, and leakage and maximum current of SC devices can be derived based on these three core parameters.

2.5. Time constant

Time constant τ is only for SC devices and defined as the product of R_{ES} and C_T as shown in **Eq. 23** using the equivalent RC circuit for a SC in **Fig. 8**. A smaller τ reflects a better responsiveness of the device, and for most of commercial SCs, τ normally ranges from 0.5 – 3.6 s [114].

$$\tau = R_{ES} \times C_T \qquad (23)$$

Based on the RC circuit model, the voltage of SC device changes by 36.8% at time $t = \tau$, and by 98% at time $t = 4\tau$, during the charge/discharge processes.

Normally τ is fixed around a certain value for SCs produced using the same technology, for example 0.55 s from Maxwell Technologies, 1.1 s from NessCap and 3.8 s from JSR Micro, as reported in [114]. Consequently, C_T and R_{ES} for the same type of SCs are inversely proportional to each other when τ is fixed. An example is shown in **Table 3** for BCAP SCs from Maxwell Technologies, and we calculated the corresponding τ values.

Table 3. C_T and R_{ES} for BCAP SCs from Maxwell Technologies.

C_T (F)	1	3.3	5	10	25	50	100	310	350	650	1200	1500	2000	3000
R_{ES} (mΩ)	700	290	170	75	42	20	15	2.2	3.2	0.8	0.58	0.47	0.35	0.29
τ (s)	0.7	0.96	0.85	0.75	1.05	1.0	1.5	0.68	1.12	0.52	0.7	0.71	0.7	0.87

Attention has to be paid here not to confuse this τ with another “relaxation time constant”,

τ_0, as occurred in [77, 115, 116]. τ_0 was proposed by Simon in [56] based on EIS test. Using the same 2.7V/1F Maxwell SC and plotting both Re(C) and Im(C) *vs*. frequency as in **Fig. 13,** τ_0 is marked at where the imaginary part of the capacitance reaches its maximum at frequency f_0, and can be calculated by **Eq. 24**:

$$\tau_0 = 1/f_0 \ = 3.86 \quad (24)$$

It is much larger than τ = 1.34 F*1.44 Ω = 1.94 s. In fact, such difference was revealed in the same paper by Simon *et al* [56]: where they reported τ = 0.7 s, but τ_0 = 10 s for their symmetric AC-based SC with mass loading of 15 mg/cm^2.

2.6. Power and energy densities

Of the performance metrics for all kinds of energy storage and conversion systems, power density and energy density are the most directly relevant to the end application and hence most often used parameters for performance evaluation.

They normally are evaluated gravimetrically or volumetrically in W/kg or W/L for power density to describe the efficacy in energy uptake/delivery; and in Wh/kg or Wh/L for energy density to demonstrate the amount of electrical energy stored or deliverable. For effective comparison with other EES devices, a Ragone plot [117] is shown in **Fig. 14**. The diagonal time line is a representative line for the so-called "characteristic time" [118], a reflection of running time of the devices at the rated power. The actual running time of EES devices varies a lot, depending on the load or discharging rate – the so-called rate dependence as discussed in 3.3 below.

Figure 14. An illustration of the power and energy densities for several EES devices via Ragone plot. The plot is based on data from Ref. [114, 119-122].

2.6.1 Power density

The outstanding power performance of SC devices is one of their major merits. The most widely used calculation method for the *maximum* power density is shown as:

$$P_D = \frac{{V_o}^2}{4\Pi R_{ES}} \qquad (25)$$

This maximum power delivery can only be realized when the load has the *identical* resistance as R_{ES}, often referred to as the *matched load* condition.

Of course in practice, the load resistor is often not matching R_{ES}. As necessary supplements, there are several other methods proposed to compute the *actual* power capacity. Three most widely adopted methods are DOE-FreedomCar [123], IEC 62576 [124] and the pulse energy efficiency (PEE) [114] methods, and one can refer to [70, 123, 125] for detailed discussions. **Table 4** provides the resulting *actual* power densities with respect to the *maximum* P_D based on the different test procedures and the data published by Burke [70, 126]. Therefore, although the maximum value P_D is widely used for comparison, one has to keep in mind that it does **NOT** usually represent the *actual* deliverable power density, and one has to choose the proper *percentage* below based on the corresponding applications.

Table 4. Power densities obtained from different methods.

	Matched load	USABC	IEC	PPE

Power density	$P_D = V_o^2/(4\Pi R_{ES})$	50% P_D	48% P_D	11.25% P_D

In principle, a further boosted P_D value is always beneficial; but little effort has been made in this [127] given the fact that SCs already have relatively high P_D.

2.6.2 Energy density

The electricity stored in or released from SCs can be evaluated through the integration of the working diagrams as illustrated in **Fig. 15** corresponding to ECLCs and PCs, where the difference in shape is caused again by their distinct charge storage mechanisms. In either case, the *stored* electric energy can be obtained from the charging curve, and the *deliverable* energy from the discharging curve. The ratio of the two is termed the *energy efficiency* of the cell, an indicator of the difference between the two parts of the curve. Calculations for the *stored* electricity are illustrated below.

a. For EDLCs or any other SCs with linear charge/discharge curves, the integration of the working diagram turns into the calculation of triangle area as shown in **Fig. 15a**, therefore:

$$E_D = \int_0^Q V_o dq = \frac{1}{2} V_o Q \qquad (26)$$

Substituting Eq. 2 into Eq. 26 yields,

$$E_D = \frac{1}{2\Pi} C_T {V_o}^2 \qquad (27)$$

Dividing by 3600 converts E_D in Joule/Π to watt hour/Π:

$$E_D = \frac{\frac{1}{2}C_T {V_o}^2}{3600 \times \Pi} \qquad (28)$$

It is worth mentioning that by combining Eqs. 23, 25 and 27, the relationship between P_D and E_D for EDLCs is given below:

$$\frac{E_D}{P_D} = 2R_{ES} \times C_T = 2\tau \qquad (29)$$

This equation indicates that the energy and maximum power densities are closely coupled by the cell time constant $\tau = R_{ES} \times C_T$. Although E_D can be increased in Eq. 27 by improving either the capacitance or operating voltage, raising the capacitance alone will simultaneously increase the time constant τ, leading to a less responsive cell, assuming R_{ES} unchanged. Whereas boosting the voltage can considerably enlarge both P_D and E_D, while still maintaining the same τ value. Also even though increasing E_D is the major stride for SC community, extra attention is required at the same time for the associated possible changes in τ or P_D.

b. However, for PCs or hybrid SCs with nonlinear charge/discharge curves as shown in **Fig. 15b**, the integration of the diagram has no simple solution, depending on the specific shape of the curve, so that:

$$E_D = \int_0^Q V dq = \int_0^{t_Q} V \times I dt \qquad (30)$$

Dividing by 3600 and Π, one can still obtain the energy density in watt hour/Π:

$$E_D = \int_0^Q V dq = \frac{\int_0^{t_Q} V \times I dt}{3600 \times \Pi} \qquad (31)$$

That is, **Eq. 28** is **NOT** valid for PCs with nonlinear charge/discharge curves, and for them **Eq. 31** has to be used.

2.7. Leakage and maximum peak currents

For SC devices, an additional yet useful parameter is the leakage current, widely used in industry to evaluate the capability of SCs to maintain the rated potential when not in use. Normally, it is recorded as the compensating current that applied to hold a fully charged SC after 72 hours.

Another similar device parameter is the maximum peak current, normally appearing in the specifications for commercial SCs. It is evaluated by discharging a fully charged SC device from V_o to ½ V_o in 1 s, and calculated as:

$$I_{max@1s} = \frac{\frac{1}{2}C_T V_o}{C_T R_{ES} + 1} \qquad (32)$$

2.8. Cycle life and capacitance retention rate

Long cycle life of SC devices is one of their major merits and leads to the so-called "fit-and-forget" benefits, highly desirable for certain applications. But this extremely long cycle life (>1,000,000 cycles) also makes it difficult to directly measure it. Another term, the *capacitance retention rate* is therefore used to indirectly estimate the cycle life of SCs. It is easily obtained in CCCD test by comparing the capacitance after given thousands of cycles with that of the first cycle. One attempt [128] was made recently by continuously test SCs for 3.8 years, and the results showed that the capacitance retention rate is decreasing almost linearly with the square root of the number of cycles. Further validations are needed to

establish this relationship, but it does give us a glimpse on the time demanding nature of the direct measurement of cycle life.

3. *Inconsistencies* in evaluation of SCs

3.1. Causes for the *inconsistencies*

For any comparison to be meaningful, the same or consistent metrics and test methods have to be used. As demonstrated and discussed in this article so far, it is easy to see why performance evaluation of SCs has become so prevalently plagued by *inconsistencies*, and where such *inconsistencies* are originated. Herein, the common causes are listed below:

a. Different instruments or calculation method used, i.e. CV, CCCD or EIS;

b. Different experiment setups:

   Three-electrode, and symmetric and asymmetric two-electrode configurations;

c. Differences in electrode fabrication:

   Mass loading, electrode thickness and density;

d. Different base *Π* used:

   Volume or mass; active material only, or combined with additives, binders; single or two electrodes; with or without electrolyte, or the whole cell;

e. Different test conditions applied (rate dependency):

   Scan rate in CV, charge/discharge current in A/g, mA/cm^2, or mA/F for CCCD tests;

The *inconsistencies* caused by the first three items on the list have been discussed in preceding sections. The effects of improper use of the base *Π* and with the rate dependency are examined below.

3.2. Device performance *vs.* material property

Although this issue has been dealt with above, the difference between device performance and material property can be huge, often overlooked, and may play a critical role in performance evaluation for any EES system. A recent paper by Gallagher *et al* [129] emphasizes such difference in the case of lithium-air batteries. To substantiate the discussion, some useful information from several SC manufacturers, including Maxwell Technologies, WIMA, Nesscap, and Ioxus [102-105], is collected and analyzed here. Owing to the fact that the mainstream SC material in industry is still activated carbon (AC), only AC-based SCs are considered.

For SC devices, their energy and power densities are summarized below:

- E_D ranges from 1 – 6 Wh/kg or 2 – 8 Wh/L;
- P_D ranges from 2 – 20 kW/kg or 4 – 30 kW/L;

The same devices but for SC materials (AC), C_S between 100 F/g and 70 F/cm^3 [62]:

- E_D ranges from 15 – 25 Wh/kg or 12 – 18 Wh/L;
- P_D ranges from 20 – 120 kW/kg or 13 – 80 kW/L;

The substantial difference between device performance and material property is clearly demonstrated above. This is due to the fact that only a small portion of the weight and

volume of SC devices are composed of active electrode materials, around 5 – 20 %, even smaller for micro-SCs [85, 94, 95]. What is worrisome is that in almost all published scientific literature [55, 60, 69, 80, 86, 130-138], no distinction has been made explicitly between the device performance and material property, leaving a room for potential misinformation and confusion.

3.3. Rate dependency

The rate dependence of all EES devices is a universal, yet thorny issue [139]. For example, batteries are usually affixed with a rated energy C_o in Ampere hour at a rated potential. However, in actual use, how much energy this battery can actually deliver to a load depends on the discharge/recharge rate [139]. In other words, if a load drains this battery in a shorter time period, the actual energy supplied will be $C_A < C_o$. Peukert's law [139, 140] is usually applied to describe this phenomena as:

$$C_A = i \cdot t = \frac{C_o}{(t_o/t)^{k-1/k}} \qquad (33)$$

And therefore the current,

$$i = \frac{C_o \cdot (t_o/t)^{k-1}}{t_o} \qquad (34)$$

Where t_o is the discharge rate or time (hrs) used to measure C_o, k is the Peukert's factor, usually $1.1 < k < 1.6$ for batteries. This k value indicates the degree of dependency of C_A on discharge rate, and a smaller value is more desirable, implying less rate independency [139].

To address this issue, the *C*-rate scheme has been proposed and widely used to scale the charge and discharge current for batteries. Different batteries are rated differently, i.e., with different k values, based on the kinetics of the battery chemistry involved. if a battery is rated

at nC, the discharging time will be fixed at around $1/n$ hours [141], i.e., if rated at 2C, for example, batteries will be completely discharged in 0.5 h. By fixing the discharge or recharge time, this C-rate system tackles successfully the issue of rate dependency for batteries with little confusion. **Fig. 16** is constructed using both **Eqs. 33** and **34** to illustrate the actual energy deliverable C_A and the electric current i, as functions of both discharge time and the C-rate level, where one can easily locate the C_A and i for a given pair of discharge time and C-rate level.

For SCs, similar rate dependency has been long and widely recognized [48, 50, 51, 65, 69, 114, 142-145], yet poorly analyzed and understood. Also similar to the C-rate system for batteries, a **60 second discharge/recharge time is recommended for SCs[146].** This 60C discharge rate or 60 s discharge/recharge time can settle the *inconsistencies* caused by the different test conditions in CCCD tests, i.e. A/g, mA/cm^2, mA/cm^3 or mA/F [130, 132, 147, 148], and can be used as a guidance to determine the proper scan rate used in CV test: v = 1/60 V/s (~16.7 mV/s) for 1 V systems; v = 2.3/60 V/s (~38.3 mV/s) for 2.3 V ones; and v = 2.7/60 V/s (45 mV/s) for 2.7 V ones.

To demonstrate the rate dependency and the use of 60 s discharge/recharge time for SCs, we collected the test data of a 1450F EDLC [11] and a 2000F hybrid SC [53] and fitted them nicely using again both **Eqs. 33** and **34** as shown in **Fig 17**. Consequently, Peukert's factor $k \approx 1.02$ is estimated for the EDLC and $k \approx 1.06$ for hybrid SC, reflecting the different kinetics of charge storage/release mechanism in each system.

5. Summary and recommendations

We identified and examined the *inconsistencies* existed in the current practice for evaluation of supercapacitors. Such *inconsistencies* are caused by some common sources including different test instruments, evaluation methods and other related factors. In summary, a fair comparison is only possible if we:

a) employ the same instruments under consistent test conditions and experimental setups;

b) derive the performance metrics using consistent calculation methods;

c) compare the comparables.

Moreover, a few more specific recommendations are proposed as followings:

1. Apply 60 seconds discharge or recharge time to address the rate dependency of supercapacitors so as to produce comparable parameters.
2. Use constant current charge/discharge (CCCD) test to determine all the three core parameters, i.e. the capacitance, equivalent series resistance and operating voltage, and subsequently the time constant, energy and power densities and leakage/maximum peak current for supercapacitor devices.
3. Use cyclic voltammetry (CV) or constant current charge/discharge (CCCD) test on a three-electrode setup to examine the operating voltage and specific capacitance of supercapacitor materials.
4. Use electrochemical impedance spectroscopic (EIS) test to study the transient impedance behavior and frequency response of supercapacitors.
5. Differentiate between the device performance and material properties, and clearly

state the mass loading, thickness, density of the electrode.

6. Pay extra attention to nonlinear charge/discharge curves when evaluating capacitance and energy performance for pseudocapacitive SCs.
7. Keep in mind the interconnections between the energy density, maximum power density and the cell time constant: they cannot be altered individually. Also note that increasing the operating voltage by using advanced electrolyte or novel cell design is the most effective way to raise both energy and power densities, while still upholding the τ value.

It is fitting to end this article by quoting from the paper by Simon et al "The prospect of developing materials with the energy density of batteries and the power density and cycle life of supercapacitors is an exciting direction that has yet to be realized. Whether to approach these goals by increasing the power density of battery materials or increasing the energy density of supercapacitors is one of the enticing features of the field. However, there needs to be clarity in the terminology used in combination with appropriate measurements and analyses. Proper evaluation of new materials and their charge storage mechanisms will facilitate progress in this important field of electrical energy storage." [146]

Acknowledgements

This work has been supported by California Energy Commission EISG Project 57470A/12-02TE, as well as by NIFA projects CA-D*-TXC-6426-RR and CA-D*-TXC-7694-H.

References

1. Erb, R.B., *Power from space for a sustainable world.* Acta Astronautica, 1997. **40**(2-8): p. 345-357.
2. Wei, X.C., et al., *SIMULATION AND EXPERIMENTAL COMPARISON OF DIFFERENT COUPLING MECHANISMS FOR THE WIRELESS ELECTRICITY TRANSFER.* Journal of Electromagnetic Waves and Applications, 2009. **23**(7): p. 925-934.
3. R., M., *Wind and solar power systems: design, analysis, and operation*. Second ed. 2012: CRC Press.
4. Rastler, D., *Electric Energy Storage Technology Options: A White Paper Primer on Applications, Costs, and Benefits*, 2010: Palo Alto, CA.
5. Martin, W. and J.B. Ralph, *What Are Batteries, Fuel Cells, and Supercapacitors?* Chem. Rev., 2004. **104**(10): p. 4245-4269.
6. Dingrando, L., K. Tallman;, and N. Hainen, *Glencoe Chemistry: Matter and Change, Chapter 21*. 2007, New York: Glencoe/McGraw-Hill.
7. Kurzweil, P., M. Chwistek, and R. Gallay, *Electrochemical and Spectroscopic Studies on Rated Capacitance and Aging Mechanisms of Supercapacitors*, in *2nd European Symposium on Super Capacitors & Applications (ESSCAP)* 2-3 November 2006: Lausanne.
8. Omanda, H., et al., *Improvement of the thermal stability of LiNi0.8Co0.2O2 cathode by a SiOx protective coating.* Journal of the Electrochemical Society, 2004. **151**(6): p. A922-A929.
9. Burke, A.F., *Materials Research for High Energy Density Electrochemical Capacitor*, in *MRS spring 2008* H.D. Abruña, M.V. Buchanan, and J.B. Goodenough, Editors. 2008. p. 1100-JJ06-02
10. Arbizzani, C., M. Mastragostino, and F. Soavi, *New trends in electrochemical supercapacitors.* Journal of Power Sources, 2001. **100**(1-2): p. 164-170.
11. Arulepp, M., et al., *The advanced carbide-derived carbon based supercapacitor.* Journal of Power Sources, 2006. **162**(2): p. 1460-1466.
12. Zhang, L.L. and X.S. Zhao, *Carbon-based materials as supercapacitor electrodes.* Chemical Society Reviews, 2009. **38**(9): p. 2520-2531.
13. Guerrero, M.A., et al., *Supercapacitors: Alternative Energy Storage Systems.* Przeglad Elektrotechniczny, 2009. **85**(10): p. 188-195.
14. Du, C.S. and N. Pan, *Supercapacitors using carbon nanotubes films by electrophoretic deposition.* Journal of Power Sources, 2006. **160**(2): p. 1487-1494.
15. Xin, Z., S.B. Mendoza, and D.P. J, *The role of nanomaterials in redox-based supercapacitors for next generation energy storage devices* NANOSCALE, 2011. **3**: p. 839-855.
16. Conway, B.E., *Transition from Supercapacitor to Battery Behavior in Electrochemical Energy-Storage.* Journal of the Electrochemical Society, 1991. **138**(6): p. 1539-1548.

17. Arbizzani, C., M. Mastragostino, and L. Meneghello, *Characterization by Impedance Spectroscopy of a Polymer-Based Supercapacitor.* Electrochimica Acta, 1995. **40**(13-14): p. 2223-2228.
18. Arbizzani, C., M. Mastragostino, and L. Meneghello, *Polymer-based redox supercapacitors: A comparative study.* Electrochimica Acta, 1996. **41**(1): p. 21-26.
19. Mastragostino, M., R. Paraventi, and A. Zanelli, *Supercapacitors based on composite polymer electrodes.* Journal of the Electrochemical Society, 2000. **147**(9): p. 3167-3170.
20. Dyatkin, B., et al., *Development of a Green Supercapacitor Composed Entirely of Environmentally Friendly Materials.* ChemSusChem, 2013.
21. Kurzweil, P. and M. Chwistek, *Electrochemical stability of organic electrolytes in supercapacitors: Spectroscopy and gas analysis of decomposition products.* Journal of Power Sources, 2008. **176**(2): p. 555-567.
22. *Ultra Capacitor - Recent Technology and Market Forecast (2020)*, 2012, SNE Research.
23. Wang, H. and L. Pilon, *Accurate Simulations of Electric Double Layer Capacitance of Ultramicroelectrodes.* The Journal of Physical Chemistry C, 2011. **115**(33): p. 16711-16719.
24. von Helmholtz, H., *Ueber einige Gesetze der Vertheilung elektrischer Ströme in körperlichen Leitern mit Anwendung auf die thierisch-elektrischen Versuche.* Ann. Phys., 1853. **165**(6): p. 211-233.
25. Helmhotz, H., *On some laws of the distribution of electrical currents in material conductors with application to experiments in animal electricity.* Pogg. Ann., 1853. **LXXXIX**: p. 211.
26. Bard, A.J. and L.R. Faulkner, *Electrochemical Methods: Fundamentals and Applications*. 2nd ed. 2000, New York: Wiley.
27. Trasatti, S. and G. Buzzanca, *Ruthenium dioxide: a new interesting electrode material. Solid state structure and electrochemical behavior.* Journal of Electroanalytical Chemistry and Interfacial Electrochemistry, 1971. **29**(2): p. App. 1-5.
28. Conway, B.E., *Electrochemical supercapacitors scientific fundamentals and technological applications*. 1999, New York: Plenum Press. 11.
29. Long, J.W., et al., *Asymmetric electrochemical capacitors—Stretching the limits of aqueous electrolytes.* MRS Bulletin, 2011. **36**(07): p. 513-522.
30. Conway, B.E., *Transition from "Supercapacitor" to "Battery" Behavior in Electrochemical Energy Storage.* J. Electrochem. Soc., 1991. **138**(6): p. 1539-1548.
31. Zheng, J.P. and T.R. Jow, *A New Charge Storage Mechanism for Electrochemical Capacitors.* J. Electrochem. Soc., 1995. **142**(1): p. L6-L8.
32. Conway, B.E., V. Birss, and J. Wojtowicz, *The role and utilization of pseudocapacitance for energy storage by supercapacitors.* Journal of Power Sources, 1997. **66**(1-2): p. 1-14.
33. Liu, T.-C., et al., *Behavior of Molybdenum Nitrides as Materials for Electrochemical Capacitors.* J. Electrochem. Soc., 1998. **145**(6): p. 1882-1888.
34. Brezesinski, K., et al., *Pseudocapacitive Contributions to Charge Storage in Highly Ordered Mesoporous Group V Transition Metal Oxides with Iso-Oriented Layered Nanocrystalline Domains.* J. Am. Chem. Soc., 2010. **132**(20): p. 6982-6990.
35. Lukatskaya, M.R., et al., *Cation intercalation and high volumetric capacitance of two-dimensional titanium carbide.* Science, 2013. **341**(6153): p. 1502-5.
36. Naoi, K. and P. Simon, *New Materials and New Configurations for Advanced Electrochemical Capacitors.* The Electrochemical Society Interface, 2008. **17**(1): p. 34-37.
37. Naoi, K., et al., *New Generation "Nanohybrid Supercapacitor".* Acc. Chem. Res., 2012. **46**(5): p. 1075-4083.
38. Arico, A.S., et al., *Nanostructured materials for advanced energy conversion and storage devices.* Nature Materials, 2005. **4**(5): p. 366-377.

39. Naoi, K., et al., *Second generation 'nanohybrid supercapacitor': Evolution of capacitive energy storage devices.* Energy & Environmental Science, 2012. **5**(11): p. 9363.
40. Cao, W.J. and J.P. Zheng, *Li-ion capacitors with carbon cathode and hard carbon/stabilized lithium metal powder anode electrodes.* Journal of Power Sources, 2013. **213**: p. 180-185.
41. Furukawa, J., et al., *Further demonstration of the VRLA-type UltraBattery under medium-HEV duty and development of the flooded-type UltraBattery for micro-HEV applications.* Journal of Power Sources, 2010. **195**(4): p. 1241-1245.
42. Cooper, A., et al., *The UltraBattery—A new battery design for a new beginning in hybrid electric vehicle energy storage.* Journal of Power Sources, 2009. **188**(2): p. 642-649.
43. Lam, L.T., et al., *VRLA Ultrabattery for high-rate partial-state-of-charge operation.* Journal of Power Sources, 2007. **174**(1): p. 16-29.
44. Lam, L.T. and R. Louey, *Development of ultra-battery for hybrid-electric vehicle applications.* Journal of Power Sources, 2006. **158**(2): p. 1140-1148.
45. Beguin, F. and E. E. Frackowiak, *Supercapacitors: Materials, Systems and Applications*. 2013, Weinheim, Germany: Wiley-VCH.
46. Khomenko, V., E. Frackowiak, and F. Béguin, *Determination of the specific capacitance of conducting polymer/nanotubes composite electrodes using different cell configurations.* Electrochimica Acta, 2005. **50**(12): p. 2499-2506.
47. Ardizzone, S., G. Fregonara, and S. Trasatti, *"Inner" and "outer" active surface of RuO_2 electrodes.* Electrochemica Acta, 1990. **35**(1): p. 263-267.
48. Kim, J.W., V. Augustyn, and B. Dunn, *The Effect of Crystallinity on the Rapid Pseudocapacitive Response of Nb2O5.* Advanced Energy Materials, 2012. **2**(1): p. 141-148.
49. Wang, X., et al., *High-Performance Supercapacitors Based on Nanocomposites of Nb_2O_5 Nanocrystals and Carbon Nanotubes.* Advanced Energy Materials, 2011. **1**(6): p. 1089-1093.
50. Brezesinski, T., et al., *Ordered mesoporous α-MoO_3 with iso-oriented nanocrystalline walls for thin-film pseudocapacitors.* Nature Materials, 2010. **9**(2): p. 146-151.
51. Wang, J., et al., *Pseudocapacitive Contributions to Electrochemical Energy Storage in TiO_2 (Anatase) Nanoparticles.* The Journal of Physical Chemistry C, 2007. **111**(40): p. 14925-14931.
52. Conway, B.E., *Electrochemical Supercapacitor: Scientific Fundamentals and Technological Applications*. 1999, New York: Plenum Publishers.
53. Burke, A. and M. Miller, *Testing of electrochemical capacitors: Capacitance, resistance, energy density, and power capability.* Electrochimica Acta, 2010. **55**(25): p. 7538-7548.
54. Miller, J.R., R.A. Outlaw, and B.C. Holloway, *Graphene double-layer capacitor with ac line-filtering performance.* Science, 2010. **329**(5999): p. 1637-9.
55. Du, C. and N. Pan, *Supercapacitors using carbon nanotubes films by electrophoretic deposition.* Journal of Power Sources, 2006. **160**(2): p. 1487-1494.
56. Taberna, P.L., P. Simon, and J.F. Fauvarque, *Electrochemical Characteristics and Impedance Spectroscopy Studies of Carbon-Carbon Supercapacitors.* Journal of The Electrochemical Society, 2003. **150**(3): p. A292.
57. Dupont, M.F., A.F. Hollenkamp, and S.W. Donne, *Large Amplitude Electrochemical Impedance Spectroscopy for Characterizing the Performance of Electrochemical Capacitors.* Journal of The Electrochemical Society, 2014. **161**(4): p. A648-A656.
58. Zhao, C., et al., *Ultrahigh capacitive performance from both $Co(OH)_2$/graphene electrode and $K_3Fe(CN)_6$ electrolyte.* Sci Rep, 2013. **3**: p. 2986.
59. Qu, D. and H. Shi, *Studies of activated carbons used in double-layer capacitors.* Journal of Power Sources, 1998. **74**(1): p. 99-107.

60. Zhu, Y., et al., *Carbon-based supercapacitors produced by activation of graphene.* Science, 2011. **332**(6037): p. 1537-41.
61. Yang, X., et al., *Liquid-mediated dense integration of graphene materials for compact capacitive energy storage.* Science, 2013. **341**(6145): p. 534-7.
62. Burke, A., *R&D considerations for the performance and application of electrochemical capacitors.* Electrochimica Acta, 2007. **53**(3): p. 1083-1091.
63. Park, J.H., et al., *An Electrochemical Capacitor Based on a $Ni(OH)_2$/Activated Carbon Composite Electrode.* Electrochemical and Solid-State Letters, 2002. **5**(2): p. H7.
64. Chen, W., et al., *Enhanced capacitance of manganese oxide via confinement inside carbon nanotubes.* Chem Commun (Camb), 2010. **46**(22): p. 3905-7.
65. Stoller, M.D. and R.S. Ruoff, *Best practice methods for determining an electrode material's performance for ultracapacitors.* Energy & Environmental Science, 2010. **3**(9): p. 1294.
66. Stoller, M., et al., *Graphene-Based Ultracapacitors.* Nano Letters, 2008. **8**(10): p. 3498-3502.
67. Qu, Q., et al., *Electrochemical Performance of MnO2 Nanorods in Neutral Aqueous Electrolytes as a Cathode for Asymmetric Supercapacitors.* Journal of Physical Chemistry C, 2009. **113**(31): p. 14020-14027.
68. Zheng, J.P., *Ruthenium Oxide-Carbon Composite Electrode for Electrochemical Capacitors.* Electrochemical and Solid-State Letters, 1999. **2**(8): p. 359-361.
69. Zhang, S. and N. Pan, *Supercapacitor performance of crumpled and planar graphene materials produced by hydrogen gas reduction of graphene oxide.* Journal of Materials Chemistry A, 2013. **1**(27): p. 7957-7962.
70. Burke, A. *Testing of Supercapacitors: Capacitance, Resistance, and Energy and Power Capacity*. in *International Symposium on Enhance Electrochemical Capacitors*. 2009. Nantes, France.
71. Fang, W., et al., *Arrayed CN_x NT–RuO_2 nanocomposites directly grown on Ti-buffered Si substrate for supercapacitor applications.* Electrochemistry Communications, 2007. **9**(2): p. 239-244.
72. Khomenko, V., E. Raymundo-Piñero, and F. Béguin, *Optimisation of an asymmetric manganese oxide/activated carbon capacitor working at 2V in aqueous medium.* Journal of Power Sources, 2006. **153**(1): p. 183-190.
73. Xu, C., et al., *Graphene-based electrodes for electrochemical energy storage.* Energy & Environmental Science, 2013. **6**(5): p. 1388.
74. Kalu, E.E., et al., *Cyclic voltammetric studies of the effects of time and temperature on the capacitance of electrochemically deposited nickel hydroxide.* Journal of Power Sources, 2001. **92**(1-2): p. 163-167.
75. Chen, Y., et al., *Electrophoretic deposition of graphene nanosheets on nickel foams for electrochemical capacitors.* Journal of Power Sources, 2010. **195**(9): p. 3031-3035.
76. Zhang, S., Y. Li, and N. Pan, *Graphene based supercapacitor fabricated by vacuum filtration deposition.* Journal of Power Sources, 2012. **206**: p. 476-482.
77. Huang, C. and P.S. Grant, *One-step spray processing of high power all-solid-state supercapacitors.* Sci Rep, 2013. **3**: p. 2393.
78. An, K.H., et al., *Electrochemical properties of high-power supercapacitors uisng single-walled carbon nanotube electrodes.* Advanced Functional Materials, 2001. **11**(5): p. 387-392.
79. Yang, Z.C., et al., *Cobalt monoxide-doped porous graphitic carbon microspheres for supercapacitor application.* Sci. Rep., 2013. **3**: p. 2925.
80. Tang, Z., C.-h. Tang, and H. Gong, *A High Energy Density Asymmetric Supercapacitor from Nano-architectured $Ni(OH)_2$/Carbon Nanotube Electrodes.* Advanced Functional Materials, 2012. **22**(6): p. 1272-1278.
81. Yan, J., et al., *Preparation of a graphene nanosheet/polyaniline composite with high specific*

capacitance. Carbon, 2010. **48**(2): p. 487-493.

82. Ryu, K.S., et al., *Symmetric redox supercapacitor with conducting polyaniline electrodes.* Journal of Power Sources, 2002. **103**(2): p. 305-309.
83. Miller, J.R. *Pulse Power Performance of Electrochemical Capacitors: Technical Status of Present Commercial Devices*. in *8th International Seminar on Double Layer Capacitors and Similar Energy Storage Devices*. 1998. Deerfield Beach, Florida.
84. Gogotsi, Y. and P. Simon, *True performance metrics in electrochemical energy storage.* Science, 2011. **334**(6058): p. 917-8.
85. Chmiola, J., et al., *Monolithic carbide-derived carbon films for micro-supercapacitors.* Science, 2010. **328**(5977): p. 480-3.
86. Zhang, J. and X.S. Zhao, *On the configuration of supercapacitors for maximizing electrochemical performance.* ChemSusChem, 2012. **5**(5): p. 818-41.
87. Yan, J., et al., *Advanced Asymmetric Supercapacitors Based on Ni(OH)$_2$/Graphene and Porous Graphene Electrodes with High Energy Density.* Advanced Functional Materials, 2012. **22**(12): p. 2632-2641.
88. Qu, D., et al., *A hydrogen-insertion asymmetric supercapacitor.* Chemistry, 2012. **18**(11): p. 3141-3.
89. Jiang, H., et al., *A green and high energy density asymmetric supercapacitor based on ultrathin MnO_2 nanostructures and functional mesoporous carbon nanotube electrodes.* Nanoscale, 2012. **4**(3): p. 807-12.
90. Yu, G., et al., *Solution-processed graphene/MnO_2 nanostructured textiles for high-performance electrochemical capacitors.* Nano. Lett., 2011. **11**(7): p. 2905-11.
91. Fan, Z., et al., *Asymmetric Supercapacitors Based on Graphene/MnO2 and Activated Carbon Nanofiber Electrodes with High Power and Energy Density.* Advanced Functional Materials, 2011. **21**(12): p. 2366-2375.
92. Park, J.H., et al., *Improved asymmetric electrochemical capacitor using Zn-Co co-doped Ni(OH)$_2$ positive electrode material.* Applied Physics A, 2005. **82**(4): p. 593-597.
93. Xiong, G., et al., *A Review of Graphene-Based Electrochemical Microsupercapacitors.* Electroanalysis, 2013: p. Early View.
94. Beidaghi, M. and Y. Gogotsi, *Capacitive energy storage in micro-scale devices: Recent advances in design and fabrication of micro-supercapacitors.* Energy & Environmental Science, 2013.
95. Pech, D., et al., *Ultrahigh-power micrometre-sized supercapacitors based on onion-like carbon.* Nature Nanotechnology, 2010. **5**(9): p. 651-654.
96. *Test Procedures for Capacitance, ESR, Leakage Current and Self-Discharging Characterizations of Ultracapacitors*, 2009, Maxwell Technologies, Inc.
97. Zhao, S., et al., *A measurement method for determination of dc internal resistance of batteries and supercapacitors.* Electrochemistry Communications, 2010. **12**(2): p. 242-245.
98. Simon, P. and A. Burke, *Nanostructured Carbons: Double-Layer Capacitance and More.* The Electrochemical Society Interface, 2008. **17**(1): p. 38-43.
99. *Supercapacitor technical guide*, Illinois Capacitors, Inc.
100. *Representative Test Procedures for Customer Evaluations*, Ioxus, Inc.
101. *Supercapacitors - Materials, Systems, and Applications*. 1 ed. New Materials for Sustainable Energy and Development, ed. M. Lu. 2013: Wiley-VCH. 446.
102. http://www.wimausa.com/.
103. http://www.nesscap.com/.
104. http://www.maxwell.com/.
105. http://www.ioxus.com/.

106. Deschamps, M., et al., *Exploring electrolyte organization in supercapacitor electrodes with solid-state NMR.* Nature Materials, 2013. **Advance online publication**.
107. Galiński, M., A. Lewandowski, and I. Stępniak, *Ionic liquids as electrolytes.* Electrochimica Acta, 2006. **51**(26): p. 5567-5580.
108. Ong, S.P. and G. Ceder, *Investigation of the Effect of Functional Group Substitutions on the Gas-Phase Electron Affinities and Ionization Energies of Room-Temperature Ionic Liquids Ions using Density Functional Theory.* Electrochimica Acta, 2010. **55**(11): p. 3804-3811.
109. Brandt, A., et al., *Ionic liquids in supercapacitors.* MRS Bulletin, 2013. **38**(07): p. 554-559.
110. Armand, M., et al., *Ionic-liquid materials for the electrochemical chanllenges of the future.* Nature Materials, 2009. **8**(8): p. 621-629.
111. Qu, Q.T., et al., *Study on electrochemical performance of activated carbon in aqueous Li_2SO_4, Na_2SO_4 and K_2SO_4 electrolytes.* Electrochemistry Communications, 2008. **10**(10): p. 1652-1655.
112. Gao, Q., et al., *Exploring the large voltage range of carbon/carbon supercapacitors in aqueous lithium sulfate electrolyte.* Energy & Environmental Science, 2012. **5**(11): p. 9611.
113. Khomenko, V., et al., *High-voltage asymmetric supercapacitors operating in aqueous electrolyte.* Applied Physics A, 2005. **82**(4): p. 567-573.
114. Burke, A. and M. Miller, *The power capability of ultracapacitors and lithium batteries for electric and hybrid vehicle applications.* Journal of Power Sources, 2011. **196**(1): p. 514-522.
115. Jang, Y., et al., *Activated carbon nanocomposite electrodes for high performance supercapacitors.* Electrochimica Acta, 2013. **102**: p. 240-245.
116. Zhi, M., et al., *Highly conductive electrospun carbon nanofiber/MnO_2 coaxial nano-cables for high energy and power density supercapacitors.* Journal of Power Sources, 2012. **208**: p. 345-353.
117. Ragone, D., *Review of Battery Systems for Electrically Powered Vehicles* 1968.
118. Christen, T. and M.W. Carlen, *Theory of Ragone plots.* Journal of Power Sources, 2000. **91**(2): p. 210-216.
119. Cairns, E.J. and P. Albertus, *Batteries for electric and hybrid-electric vehicles.* Annu Rev Chem Biomol Eng, 2010. **1**: p. 299-320.
120. Padbury, R. and X. Zhang, *Lithium–oxygen batteries—Limiting factors that affect performance.* Journal of Power Sources, 2011. **196**(10): p. 4436-4444.
121. Service, R.F., *New 'Supercapacitor' Promises to Pack More Electrical Punch.* Science, 2006. **313**(5789): p. 902-902.
122. Kötz, R. and M. Carlen, *Principles and applications of electrochemcial capacitors.* Electrochimica Acta, 2000. **45**(15-16): p. 2483-2498.
123. DOE/NE-ID-11173. *FreedomCAR Ultracapacitor Test Manual*. 2004 September 21.
124. IEC-62576, *Electric double layer capacitors for use in hybrid electric vehicles - Test methods for electrical characteristics*, 2006.
125. IEC-62391-2, *Fixed electric double layer capacitors for use in electronic equipment*, in *Part 2. Sectional specification - Electric double layer capacitors for power applications*2006.
126. Burke, A., M. Miller, and H. Zhao, *Ultracapacitors in Hybrid Vehicle Applications: Testing of New High Power Devices and Prospects for Increased Energy Density*, 2012, University of California, Daivs, Research Report UCD-ITS-RR-12-06.
127. Portet, C., et al., *Influence of carbon nanotubes addition on carbon–carbon supercapacitor performances in organic electrolyte.* Journal of Power Sources, 2005. **139**(1-2): p. 371-378.
128. Uno, M. and K. Tanaka, *Accelerated Charge-Discharge Cycling Test and Cycle Life Prediction Model for Supercapacitors in Alternative Battery Applications.* IEEE Transactions on Industrial Electronics, 2012. **59**(12): p. 4704-4712.

129. Gallagher, K.G., et al., *Quantifying the promise of lithium–air batteries for electric vehicles.* Energy & Environmental Science, 2014. **7**(5): p. 1555.
130. Zhi, M., et al., *Nanostructured carbon-metal oxide composite electrodes for supercapacitors: a review.* Nanoscale, 2013. **5**(1): p. 72-88.
131. Zheng, C., W. Qian, and F. Wei, *Integrating carbon nanotube into activated carbon matrix for improving the performance of supercapacitor.* Materials Science and Engineering: B, 2012. **177**(13): p. 1138-1143.
132. Wang, G., L. Zhang, and J. Zhang, *A review of electrode materials for electrochemical supercapacitors.* Chem Soc Rev, 2012. **41**(2): p. 797-828.
133. Tsai, W.-Y., et al., *Outstanding performance of activated graphene based supercapacitors in ionic liquid electrolyte from −50 to 80°C.* Nano Energy, 2012.
134. Lang, X., et al., *Nanoporous metal/oxide hybrid electrodes for electrochemical supercapacitors.* Nature Nanotechnology, 2011. **6**(4): p. 232-236.
135. Liu, C., et al., *Graphene-Based Supercapacitor with an Ultrahigh Energy Density.* Nano Letters, 2010. **10**(12): p. 4863-4868.
136. Hu, L., et al., *Stretchable, porous, and conductive energy textiles.* Nano Lett, 2010. **10**(2): p. 708-14.
137. Pushparaj, V.L., et al., *Flexible energy storage devices based on nanocomposite paper.* Proc. Natl. Acad. Sci. U.S.A., 2007. **104**(34): p. 13574-7.
138. Du, C. and N. Pan, *High power density supercapacitor electrodes of carbon nanotube films by electrophoretic deposition.* Nanotechnology, 2006. **17**(21): p. 5314-5318.
139. Doerffel, D. and S.A. Sharkh, *A critical review of using the Peukert equation for determining the remaining capacity of lead-acid and lithium-ion batteries.* Journal of Power Sources, 2006. **155**(2): p. 395-400.
140. Peukert, W., *Über die Abhängigkeit der Kapazität von der Entladestromstärke bei Bleiakkumulatoren.* Elektrotechnische Zeitschrift, 1897. **20**: p. 20-21.
141. Team, M.E.V., *A Guide to Understanding Battery Specifications*, December 2008.
142. Liu, J., et al., *Co_3O_4 Nanowire@MnO_2 ultrathin nanosheet core/shell arrays: a new class of high-performance pseudocapacitive materials.* Adv. Mater., 2011. **23**(18): p. 2076-81.
143. Wang, H., et al., *$Ni(OH)_2$ Nanoplates Grown on Graphene as Advanced Electrochemical Pseudocapacitor Materials.* J. Am. Chem. Soc., 2010. **132**(21): p. 7472-7477.
144. Chmiola, J., et al., *Anomalous increase in carbon capacitance at pore sizes less than 1 nanometer.* Science, 2006. **313**(5794): p. 1760-3.
145. Yun, Y.S., et al., *Microporous Carbon Nanoplates from Regenerated Silk Proteins for Supercapacitors.* Adv Mater, 2013.
146. Simon, P., Y. Gogotsi, and B. Dunn, *Where Do Batteries End and Supercapacitors Begin?* Science, 2014. **343**(6176): p. 1210-1211.
147. Biswal, M., et al., *From Dead Leaves to High Energy Density Supercapacitor.* Energy & Environmental Science, 2013.
148. Bose, S., et al., *Carbon-based nanostructured materials and their composites as supercapacitor electrodes.* Journal of Materials Chemistry, 2012. **22**(3): p. 767.
149. Luo, J., H.D. Jang, and J. Huang, *Effect of Sheet Morphology on the Scalability of Graphene-Based Ultracapacitors.* ACS Nano, 2013. **7**(2): p. 1464-1471.

Captions for Figures

Figure 1. An illustration of key performance metrics, test methods, major affecting factors for the evaluation of SCs.

Figure 2. An illustration of a typical CV test result.

Figure 3. An illustration of CCCD test result with linear potential change over time.

Figure 4. An illustration of CCCD test result with nonlinear potential change over time.

Figure 5. Schematic illustrations and equivalent circuits for different experimental setups.

Figure 6. a) Effect of mass loading and b) electrode thickness on the resulting C_S: yellow squares, green circles and purple triangles represent crumpled graphene balls, wrinkled graphene sheets, and flat graphene sheets as electrodes; and red solid squares indicate carbide-derived carbons (CDCs) as electrodes [85, 149].

Figure 7. Cyclic voltammograms of liquid-mediated graphene materials with increasing electrode density following the dashed red arrow from 0.13 – 1.33 g/cm^3 [61].

Figure 8. The series RC circuit for supercapacitors.

Figure 9. The Nyquist plot of 2.7V/1F Maxwell SC with R_{ES} determination methods marked in red.

Figure 10. CCCD result of 2.7V/1F Maxwell SC tested at different dwelling time from 0 – 30 min: (a) overall CCCD plots of one cycle; (b) averaged R_{ES} values from first six cycles; enlarged upper region of the CCCD plots at dwelling time of (c) 0 min and (d) 1 min.

Figure 11. (a) A typical CCCD plot for large SCs with *IR* drop and steady-state voltage drop marked as ΔV_1 and ΔV_2, and (b) a real case illustration of the discharge part via Skeleton Tech 1600F SC.

Figure 12. An illustration of V_o determination methods using (a) CV and (b) CCCD tests.

Figure 13. Dependence of real and imaginary capacitances over frequency for 2.7V/1F Maxwell SC with the relaxation time constant τ_o pointed.

Figure 14. An illustration of the power and energy densities for several EES devices via Ragone plot. The plot is based on data from Ref. [114, 119-122].

Figure 15. Representative working diagram from CCCD test for EDLCs (a), and PCs (b).

Figure 16. An illustration of Peukert's curve for batteries with the use of ½C marked by dashed lines.

Figure 17. An illustration of Peukert's curves for a 1450F EDLC (a) and for a 2000F hybrid SC (b) with the use of 60C marked by dashed lines.

Captions for Tables

Table 1. A chronological review of SC evaluation standards.

Table 2. Defined cell size based on cell capacitance.

Table 3. C_T and R_{ES} for BCAP SCs from Maxwell Technologies.

Table 4. Power densities obtained from different methods.